Molina Puerto, J.; Fernández Sáez, J.; Cases Iborra, FJ. (2016). Scanning electrochemical microscopy for the analysis and patterning of graphene materials: A review. Synthetic Metals. 222:145-161. doi:10.1016/j.synthmet.2016.10.019.

Scanning electrochemical microscopy for the analysis and patterning of graphene materials: a review

J. Molina[1*], J. Fernández[1], F. Cases[1]

[1]*Departamento de Ingeniería Textil y Papelera, EPS de Alcoy, Universitat Politècnica de València, Plaza Ferrándiz y Carbonell s/n, 03801 Alcoy, Spain*

Abstract

Graphene and related materials have recently emerged as outstanding materials due to a range of properties such as high mechanical strength, high electron mobility, thermal conductivity, etc. Due to their high surface area and conductivity, graphene materials have also been used for electrochemical applications such as supercapacitors, batteries, sensors, etc. Therefore, the characterization of the electroactivity of graphene materials is necessary and different electrochemical techniques such as cyclic voltammetry and electrochemical impedance spectroscopy have been widely used for this purpose. Scanning electrochemical microscopy has appeared as a unique technique that can be used to test electron transfer kinetics, electroactivity and conductivity of these materials. Even patterns can be created on graphene materials by this technique. This review aims to compile the different works performed with graphene materials and scanning electrochemical microscopy technique and provide new perspectives into the analysis of graphene materials using this technique.

Keywords: graphene, graphene oxide, patterning, electroactivity, scanning electrochemical microscopy

* Corresponding author. Fax: +34 96 652 8438; telephone: +34 966528583

E-mail addresses: jamopue@doctor.upv.es (J. Molina), jaferse1@posgrado.upv.es, fjcases@txp.upv.es (F. Cases)

Abbreviations:

AFM: Atomic force microscopy, BSA: Bovine serum albumin, CV: Cyclic voltammetry, CVD: Chemical vapor deposition, EDOT: 3,4-ethylenedioxythiophene, EIS: Electrochemical impedance spectroscopy, ERGO: Electrochemically reduced graphene oxide, FeHCF: iron (III) hexacyanoferrate (II), FETs: Field effect transistors, G: Graphene, GO: Graphene oxide, NP: Nanoparticle, Pani: Polyaniline, PDMS: Polydimethylsiloxane, PEDOT: Poly(3,4-ethylenedioxythiophene), PES: Polyester, PMMA: poly(methyl methacrylate), PPy: Polypyrrole, RGO: Reduced graphene oxide, SECM: Scanning electrochemical microscopy

1. Introduction

Since the isolation of graphene in 2004 by A.K. Geim and K.S. Novoselov [1], the number of graphene research and publications has risen dramatically. Its isolation and the groundbreaking experiments they performed with this material led to Geim and Novoselov being awarded the Nobel Prize in Physics 2010 [2]. Graphene has outstanding properties such as high electron mobility ($2.5 \cdot 10^5$ $cm^2 \cdot V^{-1} \cdot s^{-1}$), high thermal conductivity (above 3000 $W \cdot m \cdot K^{-1}$), mechanical properties (Young's Modulus (1 TPa), intrinsic strength (130 GPa), easy chemical functionalization, impermeability to gases, ability to sustain high electric current densities, optical transparency, etc. [3]. Different applications have been pointed out in the bibliography for G materials such as: photonics and optoelectronics, flexible electronics, spintronics, sensors, energy generation and storage, biomedical applications, composite materials, to name but some

[3,4]. The European Union is devoting a substantial budget (1000 million €) to graphene research with the Graphene Flagship under the Horizon 2020 programme. The aim of this research programme is "to take graphene and related layered materials from the realm of fundamental science to industrial and societal applications in the space of ten years".

The electrical conductivity and high surface area of 2630 $m^2 \cdot g^{-1}$ (theoretical value) [3] makes graphene an ideal material for electrochemical applications such as supercapacitors [5,6], batteries [6], sensors and biosensors [7,8], among others. Electrochemical properties of graphene and its electrochemical characterization has been covered in different reviews [9-12]. The techniques used for the characterization of graphene materials include CV and EIS. SECM is emerging as a unique technique that can be used for this purpose [13]. However, no review has been devoted to the characterization of G materials by this technique until now. The present review aims to fill the existing gap and provide a compilation of the work performed with SECM and G materials. This technique has been used to create patterns on graphene materials, studying electron transfer kinetics, conductivity, etc.

SECM is one of the scanning probe microscopies in which a microelectrode, as a working electrode, is positioned at an accurate distance above the substrate to obtain an appropriate response. A typical electrochemical cell consists of a microelectrode, a counter electrode and a reference electrode in a solution containing an electrolyte and the electroactive species. When a potential, sufficiently positive/negative is applied to the microelectrode, the oxidation/reduction of the electroactive species occurs at a diffusion-controlled rate on the surface of the microelectrode, and an anodic/cathodic current passes through the microelectrode. This current, $i_{T,\infty}$, attains the steady-state

quite quickly and its value depends on the electroactive species concentration, C, and its diffusion coefficient, D, according to the equation 1:

$$i_{T,\infty} = 4nFDaC \quad \text{(Equation 1)}$$

in which "n" is the number of electrons involved in the electrode reaction, F is the Faraday constant, and "a" is the radius of the microelectrode. The steady-state current results from the constant flux of electroactive species to the electrode surface driven by a hemispherical, diffusion layer around the microelectrode. In SECM, it is the perturbation of the tip current when the microelectrode tip is brought to within a few tip diameters of a surface, which constitutes the SECM response. When the tip is brought close to an insulating substrate, the steady-state current, i_T, will be smaller than $i_{T,\infty}$ because the insulating substrate partially hinders the diffusion of the electroactive species to the tip. The closer the tip is to the insulator surface, the smaller i_T is. This effect is termed "negative feedback". However, when the tip is close to a conductive substrate under a potential capable of oxidizing/reducing the electroactive species, a flux of electroactive species from the substrate in addition to the flux from the bulk solution occurs. In this case, $i_T > i_{T,\infty}$ as the distance tip/substrate decreases; this case is termed "positive feedback". Fig. 1 shows the different situations that can take place [14].

Both positive and negative feedback effects have been theoretically dealt with and it is possible to correlate experimental approach curves to analytical expressions to determine very accurately the position of the tip with respect to the substrate surface. Approach curves recorded over a conducting substrate provide an additional measurement of the effective radius of the microelectrode tip, while those recorded over insulators provide information about the effective RG (Rg/a) of the tip, where "Rg" is

the radius of the insulating part of the microelectrode and "a" is the radius of the active electrode part.

A singular aspect that makes SECM different from other electrochemical techniques, is the possibility to study unbiased samples. In this case, the potential of an unbiased substrate is not controlled by the applied voltage. On the contrary, the substrate potential, depends on the separation distance, tip potential, and other experimental factors. The total substrate current, which is the sum of the mediator regeneration current flowing at the substrate portion facing the tip and the current produced by the opposite redox reaction occurring at the substrate periphery, must equal zero at any given moment. Thus, the substrate potential continuously adjusts over the course of the feedback experiment to keep the substrate current equal to zero. This makes the feedback response at an unbiased substrate extremely sensitive to the geometry of the tip/substrate arrangement.

The comparison between the experimental approach curves I_T ($i_T/i_{T,\infty}$) vs. L (d/a) and the analytical expressions according to the theoretical model makes it possible know the electrochemical nature of the substrate. The theoretical models can be more complicated than those two limiting cases described above, which are based on pure mass transport. For example, when the rate of the $Red \rightarrow Ox + 1e^-$ reaction on the substrate is governed by the rate of heterogeneous electron-transfer kinetics rather than the rate of mass transfer (diffusion) of Red to the substrate.

The kinetics of heterogeneous electron transfer have been the focus of considerable research activity. SECM is a powerful approach for measuring the kinetics of heterogeneous electron transfer. It was commented above that SECM approach curves allow a very precise estimation of the tip–substrate distance and the tip geometric properties to be obtained, either using negative or positive feedback. In fact, both events

are limiting cases of the situation where the reaction at the substrate has a finite reaction rate. If the reaction rate is very small, regeneration of tip reactant is negligible and the substrate behaves as an inert surface, so the approach curve resembles that of hindered diffusion. In contrast, if the substrate reaction is fast enough that it operates under mass-transfer control, total positive feedback occurs and the approach curve is insensitive to the reaction rate. When the tip approaches a substrate with a finite reaction rate, the approach curve presents different degrees of feedback depending on the value of the rate constant. This sensitivity of SECM approach curves on the substrate reaction rate makes this technique a very powerful tool for the kinetics study of heterogeneous reactions.

The correlation of an experimental "kinetic-controlled" approach curve with a theoretical model allows the rate constant of the substrate reaction to be calculated. To perform this operation, models involving quasi-reversible and irreversible (reverse reaction neglected) substrate reactions governed by a single-step Butler–Volmer equation were developed [15].

Distance-dependent measurements provide quantitative information on sample properties. The main quantitative operation is obtained from the feedback mode. All values of tip current are normalized by the steady-state current, $i_{T,\infty}$, given for a disk-shaped tip electrode. The electron transfer rate can be obtained according to the corresponding formulas. These expressions are written in terms of a normalized current, $I_T = i_T / i_{T,\infty}$, and a normalized distance, L = d/a. Equations 2-7 can be used to extract the rate of heterogeneous reaction occurring at a substrate:

where I^c_T, I and I^{ins}_T represent the normalized currents for diffusion-controlled regeneration of redox mediator, finite substrate kinetics, and insulating substrate,

respectively, and I_S is the kinetically controlled substrate current, k = k·a/D, where k is the apparent heterogeneous rate constant (cm·s^{-1}) and D is the diffusion coefficient.

$$I = I_S\left(1 - \frac{I_T^{ins}}{I_T^C}\right) + I_T^{ins} \quad \text{(Equation2)}$$

$$I_T^{ins} = \frac{1}{0.15 + \frac{1.538}{L} + 0.58\exp(\frac{-1.14}{L}) + 0.0908\exp(\frac{L-6.3}{1.017\,L})} \quad \text{(Equation 3)}$$

$$I_T^C = \frac{0.78377}{L} + 0.3315\exp(\frac{-1.0672}{L}) + 0.68 \quad \text{(Equation 4)}$$

$$I_S = \frac{0.78377}{L+\frac{1}{k}} + \frac{0.68 + 0.3315\exp(\frac{-1.0672}{L})}{1 + F(L,k)} \quad \text{(Equation 5)}$$

$$F(L,k) = \frac{(\frac{11}{k\,L}) + 7.3}{110 - 40\,L} \quad \text{(Equation 6)}$$

$$k = k^0 \exp\left[\frac{(1-\alpha)\,n\,F\,(E-E^0)}{R\,T}\right] \quad \text{(Equation 7)}$$

By fitting an experimental current/distance curve to theory, the rate of an irreversible heterogeneous reaction can be obtained [15].

In addition to the amperometric feedback mode described above, other amperometric operation modes are also possible. The generation/collection (G/C) modes constitute a procedure that expands the applicability of the technique to a wider range of situations. In these modes, the collector (either tip or substrate) works as an amperometric sensor that collects the products produced at the generator surface (either substrate or tip, respectively). Thus, in the substrate generation/tip collection (SG/TC) mode, i_T is used to monitor the flux of electroactive species from the substrate and vice versa for the tip generation/substrate collection (TG/SC) mode, see Fig. 2. These methods are useful in the studies of homogeneous reactions that occur in the tip-substrate gap and also in the evaluation of catalytic activities of different materials for useful reactions. Examples of SG/TC reactions that can generate species to be detected at the tip are the generation of hydrogen at an electrode, the production of H_2O_2 from heterogeneous catalysts or the metabolites pumped out by living cell under stressing agents [15].

SECM can also be used as an imaging device, as an electrochemical tool for studies of surface reactivity of thin films and as a high-resolution fabrication tool (patterning). Due to the small size of the scanning tip, the versatility of the tip material, and various modes of operation, SECM has been used as a tool for patterning microstructures of metals and other inorganic materials, etching metals and semiconductors, electropolymerizing conducting polymers, and forming patterns of organic materials and biomolecules on a variety of substrates [16,17].

Three-dimensional SECM imaging is very useful and is obtained by scanning the tip in the XY plane and monitoring the tip and/or substrate current as a function of the tip location. This is the so-called constant height mode. The current image obtained can be converted into a plot of Z-height, i.e., d vs. XY position via a (i_T vs. L) calibration plot. For high resolution, very small tip diameters are required. The scanning in this case becomes very difficult because of the close proximity to the substrate surface. Thus, for high resolution, SECM must be carried out in the constant current mode, where the distance, d, is adjusted by a feedback loop to the z-piezo to maintain i_T constant [15].

2. Applications of SECM in graphene materials

2.1. Measurement of electroactivity

SECM technique has been used to test the electroactivity of RGO coatings [18-21] or PPy/GO coatings [22] on fabrics or RGO coatings on Pt electrodes [23]. Fig. 3-a,b shows SEM micrographs of PES fabrics coated with one RGO layer. The wrinkles of RGO sheets help to locate them on the surface of the fibers. Fig. 3-c,d shows the PES fabric after the application of 4 RGO coatings. As can be seen, all the fabric is coated with a homogeneous RGO coating. The color of the PES fabric also changed from white

to black after the application of RGO coatings. In addition, there was an improvement in conductivity as the number of RGO coatings increased [18,19]. The same happened with SECM, where an improvement in electroactivity was observed with the increasing number of RGO layers applied [18,19]. Fig. 4-a shows the approach curves to the surface of PES and PES-GO, and as can be seen, negative feedback was obtained for both samples, indicating an insulating behavior. On the other hand, when GO was reduced to RGO, a change in the trend of the approach curves was observed and a degree of positive feedback was observed (Fig. 4-b). When the number of RGO coatings applied increased, the degree of positive feedback also increased as can be seen in Fig. 4-b. The reduction of GO to RGO allows the partial restoration of the sp^2 graphitic domains, hence improving conductivity and electroactivity. In addition, amphoteric behavior was observed on the PES-RGO fabrics; the RGO coating could act either as an oxidant or a reductant with similar values of heterogeneous electron charge transfer kinetics [19].

SECM technique was also used to obtain 2-D and 3-D maps of electroactivity of the RGO-coated fabrics. Fig. 5 shows that for a sample coated with 4 RGO coatings, the fabric presented a degree of positive feedback on the whole surface. This degree of positive feedback varied from 1.19 to 1.78. The variations of the electroactivity can be attributed to a topographical effect due to the fabric structure rather than a change in the electroactivity of the coating [18,19].

Plasma treatment and BSA coating have also been applied to PES fabrics to increase the fixing of RGO. The increased electroactivity and conductivity (measured by SECM and EIS measurements, respectively), allowed the increase of RGO fixing obtained by this method [20] to be proven. The SECM technique has shown application to demonstrate the photogeneration of electrons on TiO_2/RGO coatings deposited on PES fabrics [21].

The RGO coatings improved electron transfer kinetics as shown by EIS. In another study, hybrid coatings of PPy/GO with different GO contents were deposited on PES fabrics and analyzed by the SECM technique; no substantial differences were observed in the degree of positive feedback with the increasing GO content [22]. Although Fe^{3+} redox mediator proved to be better than $Ru(NH_3)_6^{3+}$, since Fe^{3+} is sensitive to surface oxides. On the other hand, $Ru(NH_3)_6^{3+}$ is an outer sphere redox mediator and is not sensitive to surface oxides.

Molina et al. deposited ERGO on Pt electrodes and analyzed the electroactivity of the coatings by SECM with different redox mediators [23] (Fig. 6). A similar degree of positive feedback was obtained with $Ru(NH_3)_6^{3+}$ and $Fe(CN)_6^{3-}$ redox mediators (1.7-1.8), however with the Fe^{3+} redox mediator, slight degree of positive feedback or even negative feedback was observed. This could be due to the reaction between Fe^{3+} ions with RGO coating.

Azevedo et al. [24] used the SECM technique to map the conductivity of GO films deposited on glass based on feedback current; the reduction of GO films by NaOH was also studied. A mathematical formula based on a model was applied to convert the feedback current to conductivity. The technique was contactless and avoided damaging of the coating. However, careful selection of the analysis parameters was needed in order to maximize the response. In particular, the redox solutions used for the measurements had both FcMeOH and $FcMeOH^+$ (FcMeOH was produced by electrolysis of FcMeOH), the microelectrode had a RG = 3 (12 μm radius Pt probe). A more concentrated solution was used to map the more conductive situation in order to have dimensionless conductivity (σ*) values that were mostly within the 0.2−2 range. Fig. 7-a shows a SECM 2-D scan of a GO coating on SiO_2/Si substrate prior to NaOH exposure. Fig. 7-b shows a zone of the sample after exposure to 0.1 M NaOH for 30 s.

As can be seen, there was an increase in the measured feedback current due to a better conductivity of the coating produced by the reduction produced by NaOH. Fig. 7-c and Fig. 7-d show the same graphs after conversion to conductivity by means of the mathematical model proposed by the authors.

Wain et al. [25] fabricated probes for SECM-AFM combined measurements performed on exfoliated G samples. A Pt nanoelectrode was surrounded by a layer of silicon nitride, focused ion beam and etching techniques were combined in the fabrication process. Surface topography was recorded by AFM technique in contact mode and subsequently, SECM measurements were performed at a surface height of 150 nm. Fig. 8 shows a comparison of AFM profiles (a, c, e, g) and SECM imaging (b, d, f, h) of different G flakes. Circular zones of low electroactivity were observed in the graphitic areas which do not have correlation with the AFM profiles. These zones could be linked to the adsorption of blocking adsorbates or intrinsic chemical impurities in the carbon. A line profile was applied in Fig. 8-g and 8-h and the results are shown in Fig. 8-i. Zones where single-layer G was present showed a height of 0.4 nm; however multilayer G and few-layer G zones were also observed with AFM. SECM imaging, however showed little difference between the different zones. It should be taken into account that bias was not applied, and current could be close to transport limited.

Reiner-Rozman et al. [26] produced FETs based on RGO coatings on SiO_2/Si. RGO coatings acted as p-type semiconducting materials and the FETs were used in pH titration, where a slope of 6.1 μA/pH and a noise level of 100 nA were obtained, which served to distinguish pH differences of 0.02. The SECM technique was used to characterize the degree of coverage and the effective reduction of GO to RGO in the constant distance mode. The SECM technique is able to analyze larger surface areas than XPS or Raman, whose analysis is focused on a small area. SiO_2 and GO surfaces

showed negative feedback since they are insulating materials that are not able to reduce the oxidized form of the redox mediator (redox current between 120-200 pA). However, when GO was reduced to RGO a substantial increase of the oxidation current on the microelectrode was measured (400-650 pA), indicating that the substrate is an electroactive material that is able to reduce the redox mediator. The degree of coverage of RGO could be calculated by means of 2-D and 3-D representations. In this way, the SECM technique served as a probe technique to test the characteristics of chemically obtained RGO coatings.

Bourgeteau et al. [27] performed a study with SECM in which they evaluated the contact resistances of RGO flakes in addition to the intrinsic resistance of RGO flakes. The method used consisted of using different redox mediator concentrations and the measurement of the microelectrode current. With the help of numerical simulation, the authors were able to isolate the different contributions. The size of the flakes had an influence on the response obtained. Higher flake size allows a higher area on which the counter reaction can take place, this enhances the redox flux and a higher increase in current is obtained. In the same way, overlapping between RGO flakes produces an increase of the area, which enhances the current increase. On the other hand, lowest currents are obtained on isolated flakes. Fig. 9-a shows a SEM micrograph of different RGO flakes, interconnected or not, and the corresponding SECM representation obtained (Fig. 9-b). As can be seen the flake α produces the highest currents due to its larger size. The flakes in contact with it, β and β', also show a large increase in current due to the interconnection with α flake. However, isolated flakes with lower size and interconnection, γ and γ', show a lower increase in current. Fig. 9-c shows schematic representation of the reactions that take place, where the interconnections allow a higher area in which counter reaction can take place.

To determine the electrical resistances, the electroactivity of the flakes was measured with different redox mediator concentrations (Fig. 10). Increasing the redox mediator concentration led to a decrease in the SECM response, since solicitation increased and the substrate had to transport more electrons to sustain the feedback loop. With the increase in the concentration of the redox mediator, the electronic communication between flakes begins to be a limiting factor and the response is merely brought about by the conductivity of the analyzed zone and is not dependent on flake size and their interconnections. The results obtained were analyzed with theoretical models and simulations. Individual flakes showed a resistance of 30 MΩ which, taking into account the thickness of the flake, led to a conductivity of 0.2 $S \cdot cm^{-1}$. The intrinsic resistance for interconnected flakes was the same as for isolated flakes (30 MΩ), however the contact resistance was about five orders of magnitude higher (150 MΩ). Thus, the interflake resistance limits the electron transport of RGO-based materials.

Rapino et al. [28] analyzed GO and RGO flakes on Au and SiO_x substrates, respectively. On Au substrates, only the redox mediator $K_4Fe(CN)_6$ allowed a clear contrast between the conducting Au and insulating GO flakes. Au was able to reduce the oxidized form of the mediator; GO was not able to do this (negative feedback on GO). GO and $K_4Fe(CN)_6$ presented negative charge and repulsion between them did not allow charge transfer. FcMeOH and $Ru(NH_3)_6Cl_3$ redox mediators did not allow a clear contrast between GO and substrate material, since the oxidation of both redox mediators at the substrate surface was similar on Au and GO. On the other hand, FcMeOH and $Ru(NH_3)_6Cl_3$ redox mediators allowed the contrast between conducting RGO and insulating SiO_2 substrate since they were oxidized on the substrates with different rates. Conversely, the redox mediator $K_4Fe(CN)_6$ was not reduced either on the SiO_2 or on the RGO, since repulsion between negative charges of the redox mediator and both surfaces

took place. Hence, selecting an appropriate substrate and redox mediator, taking into account the electrostatic interactions that are going to take place, is crucial for observing G materials by the SECM technique. Following these premises, two other redox mediators with negative charge (FcCOOH and $Na_3(IrCl_6)$) were used to study its behavior on Au/GO substrates. The best results were obtained with the second one, since it presented three negative charges instead of one negative charge for FcCOOH.

Tan et al. [29] studied the reactivity of CVD monolayer G and imperfections generated on its surface by mechanical and chemical damage. These defects can strongly influence the electrical, chemical, and mechanical characteristics of graphene. G defects are generally classified as intrinsic and extrinsic. Intrinsic defects are structural defects, for example, vacancies, carbon ad-atoms, Stone-Wales defects, and grain boundaries. Extrinsic defects are the result of the introduction of foreign atoms. To examine the CVD graphene imperfections by SECM, $K_3Fe(CN)_6$ was selected as the redox mediator because it provides good contrast between the electrochemical activity of the defect sites and G. The variations in feedback current indicated that the defects sites had very different electron transfer kinetics compared to the overall graphene surface. Defects were introduced by deliberate mechanical damage (Fig. 11) and by chemical oxidation with NaOCl (Fig. 12). The electrochemical activity of the mechanically damaged surface was scanned and the SECM image is shown in Fig. 11-b. The defects could be passivated by means of electropolymerization of o-phenylenediamine (OPD) (Fig. 11-c).

The defects were also induced chemically, as observed in Fig. 12-a. The electropolymerization of OPD also allowed the chemically created defects to be passivated (Fig. 12-b). The authors also studied the effect of the carboxylic group functionalization with aminoferrocene.

The electroactivity of catalytic materials containing G-derivatives, used for H_2O_2 determination, has been also monitored by means of SECM [30,31]. Castro Júnior et al. [30] produced RGO-PEDOT-FeHCF/Au electrodes for the amperometric determination of H_2O_2. SECM technique was used to test the electroactivity of RGO-PEDOT-FeHCF/Au and PEDOT-FeHCF/Au electrodes using the reduction of $Fe(CN)_6^{3-}$ on the substrate as the monitoring reaction. The electroactivity was higher on the RGO/PEDOT/FeHCF surface owing to the uniform incorporation of FeHCF mediator molecules and enhanced electron transfer due to the presence of RGO. In addition, RGO produced a 3-D structure that avoided the aggregation of the other components. The performance of the electrodes for H_2O_2 determination was also greatly improved with the presence of RGO. The work developed by Justino et al. [31] followed the same orientation as the previous work, however in this case, SECM was used for real-time mapping of H_2O_2 concentration during electrochemical reduction of oxygen. For this purpose, the developed electrode was moved above a Pt electrode generating H_2O_2 to map its generation. In addition, the authors performed a kinetic study varying the substrate potential and registering approaching curves. With this experiment, the authors obtained apparent heterogeneous electron transfer constant (k_{app}) values, as a function of substrate potential and calculated the heterogeneous rate constant (k^0). The rate constant for RGO/PEDOT/FeHCF was $7.5 \cdot 10^3$ $cm \cdot s^{-1}$, higher than for other combinations of electrode materials. This increase in the rate constant can be attributed to RGO conductivity which enhances the electron transfer between the active material and the electrode, in addition a better distribution of FeHCF catalyst was promoted.

Gupta and co-workers used the SECM technique to characterize G-based materials for supercapacitor applications [32,33]. In [32], the authors synthesized PPy/GO and Pani/GO by electrochemical layer-by-layer assembly. Using electrochemical reduction,

PPy/ERGO and Pani/ERGO composites were also obtained. ERGO nanosheets provided high surface area and conductivity and PPy and Pani provided their redox reactions to increase the capacitance of the electrodes. Electroactivity of the electrodes was scanned with the tip generation/substrate collection mode to map surface ion adsorption. Pani electrodes were more electroactive than PPy ones. ERGO containing electrodes were more electroactive than GO ones due to the increased conductivity of ERGO. GO/MnO_2 and RGO/MnO_2 hybrid materials have been also characterized by SECM [33].

2.2. Measurement of heterogeneous electron transfer rate constants

Chen et al. [34] observed high values of heterogeneous electron transfer kinetics on G grown by CVD. The authors avoided coating the side of the G sheet to be analyzed with PMMA or polystyrene to avoid contamination. Instead, the other side of the G sheet, was coated with PMMA or alternatively, polystyrene. To demonstrate the ultrafast electron transfer kinetics, the authors used SECM-based nanogap voltammetry and studied oxidation and reduction of the FcMeOH under high-mass transport conditions, either with the substrate-generation/tip-collection or the feedback mode with small nanogaps between microelectrode and G surface (Fig. 13). The authors obtained values of k^0 around 1.6 $cm \cdot s^{-1}$ for PMMA-supported G (25-100 times higher than in the bibliography due to the fact that PMMA contamination which affects G electroactivity was avoided). The reduction of the oxidized redox mediator form ($FcMeOH^+$) was affected by the polar and positive charged PMMA below the G coating, which made the electron transfer difficult, as stated by the authors. The oxidation process was not affected, since the redox mediator is in its neutral form (FcMeOH). When using polystyrene (neutral and nonpolar) instead of PMMA, the authors obtained higher

values of k^0 in the order of 25 $cm \cdot s^{-1}$. Thus the supporting material affects the electron transfer kinetics. In addition, the authors pointed out the need to avoid hydrophobic airborne contamination.

Xie et al. [35] deposited a self-assembled monolayer on Au electrode. This layer blocked electron transfer between Au and the redox solution. On top of the self-assembled monolayer, G nanosheets were adsorbed by means of hydrophobic interaction and π-conjunction. Electron transfer was reestablished due to the electroactivity of G, which facilitated electron transfer with the redox mediator and in addition facilitated tunneling between G and Au through the self-assembled monolayer. The apparent heterogeneous rate constant was evaluated by means of approach curves obtained with SECM and the value obtained was equal to $6.8 \cdot 10^{-2}$ $cm \cdot s^{-1}$.

Ritzert et al. [36] used different redox mediators in aqueous and non-aqueous media to investigate the heterogeneous electron transfer kinetics of G grown by CVD. The method used was feedback mode and approach curves. The adjustment to the theoretical model was performed in order to determine the heterogeneous electron transfer rate constant. Fig. 14 shows the cyclic voltammograms of the different redox mediators used in the work on a Pt microelectrode.

The different redox mediators, analyzed in aqueous media, comprised three categories. $[Fe(CN)_6]^{3-}$, $[Fe(CN)_6]^{4-}$, $[Ru(CN)_6]^{4-}$, $[Mo(CN)_8]^{4-}$, and Fe(III)EDTA exhibited quasi-reversible kinetics. These redox mediators showed approach curves that changed with the applied potential to the electrode, negative feedback at open circuit potential and ill-defined peaks in CV. FcMeOH and CoSep showed a degree of positive feedback at open circuit potential and at all the potentials applied to the electrode, which indicated faster kinetics than the previous redox mediators. An overpotential was necessary to achieve diffusion-controlled positive feedback, hence the kinetics of these redox

mediators was not completely reversible on the surface of G. $[Ru(bpy)_3]^{2+}$, $[Ru(NH_3)_6]^{3+}$, and MV, always gave positive feedback, which was not potential dependent, suggesting reversible kinetics at G. The different heterogeneous electron transfer rate constants and diffusion coefficients obtained for the different redox mediators have been included in Table 1.

The authors also modified G with a partial monolayer of Osdipy complex through simple adsorption as a way to increase the electroactivity of the electrode without affecting the conductivity of G. The electron transfer kinetics of quasi-reversible mediators, Fe(III)EDTA and $[Ru(CN)_6]^{4-}$, was enhanced due to the presence of Osdipy. This could be used to detect small amounts of adsorbed species on G.

2.3. Measurement of diffusion coefficients of adsorbates on graphene

Rodríguez-López et al. [37] studied the diffusion of a cobalt bis-terpyridine, Co(tpy)2-containing tripodal compound (1·2PF6) which was designed to adsorb onto the surface of single-layer G without non-covalent interactions through three pyrene moieties. The compound was deposited on certain spots and the electroactivity evolution with time was measured with substrate generation/ tip collection and feedback modes. In the oxygen reduction region, the tripodal compound generates more H_2O_2 than G. H_2O_2 was analyzed temporally and spatially. The tripodal compound also mediated with the Fe^{2+} species generated at the SECM tip. In both cases, the electroactivity was studied under conditions where G showed less activity than the tripodal compound in order to study only the diffusion of the tripodal compound. With both modes of analysis, there was a gradual decrease in electroactivity due to the radial diffusion of the tripodal compound outside the spots where it was originally deposited. The response was fitted to a surface

diffusion model to calculate the diffusion coefficients. The non-covalent modification allowed enhancement of the electroactivity of G without losing its electronic properties.

2.4. Creation of patterns

In the family of G materials, GO has several advantages over G, since it can be produced in larger amounts due to the fabrication process that involves oxidation, and is cheaper for this reason [38]. GO can also be easily dispersed in aqueous solutions due to the negative charges of its structure which stabilize its dispersions and improve processability [39]. Such a good dispersability favors its deposition on different surfaces. G production by mechanical cleavage produces a high quality material, however production using this method is very small and it is only used for laboratory experiments. CVD has been also used to produce high quality G, however the process is more complex and expensive. Although GO is cheaper, it is a semiconducting material and if more conductivity is needed, a reduction process must be used [40,41]. Reduction methods include chemical, thermal, UV, and electrochemical methods. With the electrochemical methods, no additional chemicals are used, since the reactive is the electron provided by means of electrochemical techniques. When reducing GO to RGO, conductivity is gained due to a partial restoration of the graphitic sp^2 structure [40,41].

Chemical methods of reduction are non-selective and all the surface of the material treated is reduced. On the other hand, the creation of patterns is of interest for creating electrical circuits for G-based devices, sensors, etc. UV methods and thermal methods have been applied for zonal reduction. Similarly, the SECM technique has been also used for the creation of these patterns [42-44]. Two of the works used GO as the G precursor and reduced to RGO by means of the SECM technique [42,43]. The reduction

was carried out selectively on the zone where the microelectrode passed above the sample.

Liu et al. [42] used a Pt microelectrode located at ~12 μm above a stainless steel electrode and a negative potential was applied to the stainless steel electrode. Between the microelectrode and the substrate, a GO solution was located. The negative potential applied produced the reduction of GO to RGO on the stainless steel surface due to the confined electrical field. Patterns were created by moving the microelectrode laterally at different reduction potentials and different scan rates. Fig. 15 shows the patterns obtained by applying a different reduction potential. Fig. 15-a shows the SEM micrographs of the patterns. Fig. 15-b shows a magnified SEM micrograph that shows the crumpled surface of RGO. Finally, Fig. 15-c and Fig. 15-d show the EDX mapping of C and O, respectively. As can be seen, when applying a reduction potential of -4.5 V (vs. tip), total coverage of the surface of the pattern was obtained (line 2), and the width and thickness of the pattern at this potential was 53 μm and 320 nm, respectively. Authors did not observe deposition when the applied potential was more positive than -4 V. Regarding the influence of the scan rate, no differences were observed when varying the scan rate below 10 $\mu m \cdot s^{-1}$. However, scan rates higher than 30 $\mu m \cdot s^{-1}$ did not allow clear patterns to be obtained.

The obtained patterns were characterized towards the catalysis of dopamine redox reactions (Fig. 16). A positive potential (0.8 V) was applied on the microelectrode to oxidize dopamine, which was reduced on the surface of RGO. The current obtained was higher on RGO surface than on stainless steel one, which indicates higher electroactivity of RGO film. The signal was also higher in the case of employing lower scan rates during the synthesis of the RGO film as can be seen in Fig. 16. This

patterning technique could be used, in principle, on any conducting substrate, and Au electrodes were also tested as substrate materials.

Azevedo et al. [43] deposited GO on a SiO_2 substrate. Thereafter, naphtalene radical anions were electrogenerated on the surface of the microelectrode at -2.6 V (vs. SCE), and these species diffused to the substrate surface where they were able to reduce GO to RGO. When using a 10 μm microelectrode, the width of the patterns obtained was around 50 μm. When a lower diameter microelectrode tip (1 μm diameter) was used, the width of the patterns was 8 ± 3 μm (400 $\mu m \cdot s^{-1}$) and 18 ± 5 μm (1 μm diameter tip, 100 $\mu m \cdot s^{-1}$). Hence, the lower the diameter of the microelectrode tip, the narrower the width of the pattern. The employment of higher scan rates also allowed a decrease of the width of the pattern. Fig. 17-a shows a pattern obtained after reducing GO with this method. The patterns created were connected with Au electrodes and a negative potential was applied to produce the electrografting of a diazonimum salt (4-aminoethylbenzenediazonium). The salt was fixed through covalent bonding after the generation of aryl radicals. Therafter, the self-assembly of AuNPs was produced through simple dipping in a solution containing citrate coated AuNPs (negative charge) and NPs were fixed through electrostatic interaction. Fig. 17-b shows an AFM image of the AuNPs on the diazonium/RGO coating. Fig. 17-c,d show SEM micrographs of the AuNPs.

Torbensen et al. [44] used the SECM technique to produce carboxylation patterns on multilayered G coated on Ni substrate. Carboxylates are versatile linkers than can be further modified. The SECM technique operated in the direct mode and a -2.6 V voltage was applied to the G electrode to reduce the CO_2 to $CO_2^{\bullet -}$, which could either dimerize to $C_2O_4^{2-}$ (oxalate) or react with G surface and produce the carboxylation of its surface. Different electrolysis times (5, 10 and 30 s) were applied on different spots. The result

was the creation of patterns of carboxylated G which were analyzed by means of SECM technique in a solution containing ferrocene as the redox mediator. As can be observed in Fig. 18, a change in the time of electrolysis form 5 to 10 s produced an increase of the carboxylated surface. However, higher time of electrolysis (up to 30 s) had little effect, as observed by SECM, although XPS analyses showed an increase of the O-C=O groups with the increasing electrolysis time.

Carboxylation produced a decrease of the conductivity in the zones where it was applied, so that the normalized current suffered a decrease from 1.6 for bare G to 1.1 for carboxylated G. The diameter of the patterns created was 57, 78 and 83 μm for 5, 10 and 30 s of electrolysis, respectively. The authors pointed out the need to limit the time of electrolysis to 5 s in order to avoid other reactions (hydroxyl and carbonyl groups) and not introduce severe disruptions on G.

3. Conclusions and perspectives

The scanning electrochemical microscopy technique is being increasingly used for the characterization of graphene materials. One of the main advantages of this technique is that it does not damage the sample since there is no contact between the tip, where the redox processes are measured, and the sample. In addition, samples can be analyzed at their open circuit potential, with no imposed potential. Among its different modes of operation, feedback mode is the most used. From this method, approach curves that give information on electroactivity and electron transfer rate kinetics can be obtained. The technique also allows 2-D and 3-D maps of electroactivity to be obtained which are very useful to characterize the electroactivity of graphene materials over a relatively large surface area, when compared with AFM techniques for example. Depending on the sample, substrate and their interactions, different redox mediators can be used. Hence,

the redox mediator and its concentration should be carefully selected depending on what is wanted from this technique. SECM technique has been used to characterize graphene materials applied to produce conductive fabrics, supercapacitors, field effect transistors, sensors, electrode materials, etc. SECM can also be used to detect contamination on graphene materials since the electroactivity measured (heterogeneous electron transfer rate kinetics, etc.) is very sensitive to organic contamination. Its versatility has been also demonstrated since it can be used to create patterns of graphene materials using graphene oxide as a precursor or functionalize graphene materials previously deposited with patterns (carboxylation and diazonium modifications have been reported, but other types of functionalization will be certainly explored in the future with this technique). The electrochemical data can be converted to conductivity employing models, which is very useful to characterize also the conductivity of graphene materials. However, the work performed is still limited and there is potential for the growth of this technique applied to the study of 2-D materials. The characterization of other graphene derivatives such as nitrogen doped graphene [45-47], metallic doped graphene [48] or other forms of doping (such as B, P, S, F, Cl, Br, I, Se, etc.) [49] has not still been reported and it is an area of future study that will be certainly explored. At present, other 2-D materials such as transition metal dichalcogenides is an area of intense study in the materials science and physics field [50-53]. However, the SECM technique has still not been applied to the study of these materials.

Acknowledgements

Authors wish to thank to the Spanish Ministerio de Ciencia e Innovación (contract MAT2016-77742-C2-1-P) for the financial support. J. Molina is grateful to the Conselleria d'Educació, Formació i Ocupació (Generalitat Valenciana) for the Programa

VALi+D Postdoctoral Fellowship (APOSTD/2013/056). Tim Vickers is gratefully acknowledged for help with the English revision.

Role of the founding source

The founding sources had no any involvement in study design; in the collection, analysis and interpretation of data; in the writing of the report; and in the decision to submit the article for publication.

References:

[1] K.S. Novoselov, A.K. Geim, S.V. Morozov, D. Jiang, Y. Zhang, S.V. Dubonos, I.V. Grigorieva, A.A. Firsov, Electric Field Effect in Atomically Thin Carbon Films, Science 306 (2004) 666–669.

[2] A.K. Geim, Random Walk to Graphene (Nobel Lecture), Angew. Chem. Int. Ed. 50 (2011) 6967–6985.

[3] K. S. Novoselov, V. I. Fal'ko, L. Colombo, P. R. Gellert, M. G. Schwab, K. Kim, A roadmap for graphene, Nature 490 (2012) 192-200.

[4] A.C. Ferrari, et al., Science and technology roadmap for graphene, related two-dimensional crystals, and hybrid systems, Nanoscale 7 (2015) 4598–4810.

[5] Y. Shao, M.F. El-Kady, L.J. Wang, Q. Zhang, Y. Li, H. Wang, M.F. Mousaviae, R.B. Kaner, Graphene-based materials for flexible supercapacitors, Chem. Soc. Rev. 44 (2015) 3639–3665.

[6] R. Raccichini, A. Varzi, S. Passerini, B. Scrosati. The role of graphene for electrochemical energy storage, Nat. Mater. 14 (2015) 271–279.

[7] E.B. Bahadır, M.K. Sezgintürk, Applications of graphene in electrochemical sensing and biosensing, Trends Anal. Chem. 76 (2016) 1–14.

[8] D. Zheng, H. Huc, X. Liu, S. Hu, Application of graphene in electrochemical sensing, Curr. Opin. Colloid In. 20 (2015) 383–405.

[9] M. Pumera, Electrochemistry of graphene, graphene oxide and other graphenoids: Review, Electrochem. Commun. 36 (2013) 14–18.

[10] M. Pumera, Graphene-based nanomaterials and their electrochemistry, Chem. Soc. Rev. 39 (2010) 4146–4157.

[11] D.A.C. Brownson, C.E. Banks, Graphene electrochemistry: an overview of potential applications, Analyst 135 (2010) 2768–2778.

[12] D.A.C. Brownson, D.K. Kampouris, C.E. Banks, Graphene electrochemistry: fundamental concepts through to prominent applications, Chem. Soc. Rev. 41 (2012) 6944–6976.

[13] N. Ebejer, A.G. Güell, S.C.S. Lai, K. McKelvey, M.E. Snowden, P.R. Unwin, Scanning Electrochemical Cell Microscopy: A Versatile Technique for Nanoscale Electrochemistry and Functional Imaging, Annu. Rev. Anal. Chem. 6 (2013) 329–351.

[14] P. Sun, F.O. Laforge, M.V. Mirkin, Scanning electrochemical microscopy in the 21st century, Phys. Chem. Chem. Phys. 9 (2007) 802–823.

[15] F. Ren, F. Fan, J. Fernandez, B. Liu, J. Mauzeroll, Scanning Electrochemical Microscopy, in: C.G. Zoski (Eds.), Handbook of Electrochemistry, Elsevier B.V., 2007, pp. 471-549.

[16] D. Mandler, Micro and nanopatterning using the scanning electrochemical microscope, in: A.J. Bard, M.V. Mirking (Eds.), Scanning Electrochemical Microscopy, Marcel Dekker, New York, 2001, pp. 593–627.

[17] B.R. Horrocks, Encyclopedia in Electrochemistry, in: A.J. Bard, M. Stratmann, P.R. Unwin (Eds.), Instrumentation and Electroanalytical Chemistry, Wiley-VCH Verlag GmbH., Weinheim, 2003, pp. 444–490.

[18] J. Molina, J. Fernández, J.C. Inés, A.I. del Río, J. Bonastre, F. Cases, Electrochemical characterization of reduced graphene oxide-coated polyester fabrics, Electrochim. Acta 93 (2013) 44–52.

[19] J. Molina, J. Fernández, A.I. del Río, J. Bonastre, F. Cases, Chemical and electrochemical study of fabrics coated with reduced graphene oxide, Appl. Surf. Sci. 279 (2013) 46–54.

[20] J. Molina, J. Fernández, M. Fernandes, A.P. Souto, M.F. Esteves, J. Bonastre, F. Cases, Plasma treatment of polyester fabrics to increase the adhesion of reduced graphene oxide, Synth. Met. 202 (2015) 110–122.

[21] J. Molina, F. Fernandes, J. Fernández, M. Pastor, A. Correia, A.P. Souto, J.O. Carneiro, V. Teixeira, F. Cases, Photocatalytic fabrics based on reduced graphene oxide and TiO_2 coatings, Mat. Sci. Eng. B-Solid 199 (2015) 62–76.

[22] J. Molina, A. Zille, J. Fernández, A.P. Souto, J. Bonastre, F. Cases, Conducting fabrics of polyester coated with polypyrrole and doped with graphene oxide, Synth. Met. 204 (2015) 110–121.

[23] J. Molina, J. Fernández, C. García, A.I. del Río, J. Bonastre, F. Cases, Electrochemical characterization of electrochemically reduced graphene coatings on platinum. Electrochemical study of dye adsorption, Electrochim. Acta 166 (2015) 54–63.

[24] J. Azevedo, C. Bourdillon, V. Derycke, S. Campidelli, C. Lefrou, R. Cornut, Contactless Surface Conductivity Mapping of Graphene Oxide Thin Films Deposited on Glass with Scanning Electrochemical Microscopy, Anal. Chem. 85 (2013) 1812−1818.

[25] A.J. Wain, A.J. Pollard, C. Richter, High-Resolution Electrochemical and Topographical Imaging Using Batch-Fabricated Cantilever Probes, Anal. Chem. 86 (2014) 5143−5149.

[26] C. Reiner-Rozman, J. Schodl, C. Nowak, C. Kleber, Scanning Electrochemical Microscopy as a Characterization Tool for Reduced Graphene Oxide Field Effect Transistors, e-J. Surf. Sci. Nanotechnol. 13 (2015) 366−372.

[27] T. Bourgeteau, S.L. Vot, M. Bertucchi, V. Derycke, B. Jousselme, S. Campidelli, R. Cornut, New Insights into the Electronic Transport of Reduced Graphene Oxide Using Scanning Electrochemical Microscopy, J. Phys. Chem. Lett. 5 (2014) 4162−4166.

[28] S. Rapino, E. Treossi, V. Palermo, M. Marcaccio, F. Paolucci, F. Zerbetto, Playing peekaboo with graphene oxide: a scanning electrochemical microscopy investigation, Chem. Commun. 50 (2014) 13117-13120.

[29] C. Tan, J. Rodríguez-López, J.J. Parks, N.L. Ritzert, D.C. Ralph, H.D. Abruña, Reactivity of Monolayer Chemical Vapor Deposited Graphene Imperfections Studied Using Scanning Electrochemical Microscopy, ACS Nano 6 (2012) 3070–3079.

[30] J.G.M. Castro Júnior, G.M.M. Ferreira, F.G. de Oliveira, F.S. Damos, R.d.C.S. Luz, A novel platform based on graphene/poly(3,4-ethylenedioxythiophene)/ iron (III) hexacyanoferrate (II) composite film for electrocatalytic reduction of H_2O_2, J. Electroanal. Chem. 732 (2014) 93–100.

[31] D.D. Justino, I.L. Torres, R.d.C.S. Luz, F.S. Damos, High Sensitive Microsensor Based on Organic-Inorganic Composite for Two-Dimensional Mapping of H_2O_2 by SECM, Electroanal. 27 (2015) 1202–1209.

[32] S. Gupta, C. Price, Scanning electrochemical microscopy of graphene/polymer hybrid thin films as supercapacitors: Physical-chemical interfacial processes, AIP Adv. 5 (2015) 107113.

[33] S. Gupta, M. van Meveren, J. Jasinski, Investigating Electrochemical Properties and Interfacial Processes of Manganese Oxides/Graphene Hybrids as High-Performance Supercapacitor Electrodes, Int. J. Electrochem. Sci. 10 (2015) 10272–10291.

[34] R. Chen, N. Nioradze, P. Santhosh, Z. Li, S.P. Surwade, G.J. Shenoy, D.G. Parobek, M.A. Kim, H. Liu, S. Amemiya, Ultrafast Electron Transfer Kinetics of Graphene Grown by Chemical Vapor Deposition, Angew. Chem. Int. Ed. 54 (2015) 15134–15137.

[35] X. Xie, K. Zhao, X. Xu, W. Zhao, S. Liu, Z. Zhu, M. Li, Z. Shi, Y. Shao, Study of Heterogeneous Electron Transfer on the Graphene/Self-Assembled Monolayer Modified Gold Electrode by Electrochemical Approaches, J. Phys. Chem. C 114 (2010) 14243–14250.

[36] N.L. Ritzert, J. Rodríguez-López, C. Tan, H.D. Abruña, Kinetics of Interfacial Electron Transfer at Single-Layer Graphene Electrodes in Aqueous and Nonaqueous Solutions, Langmuir 29 (2013) 1683−1694.

[37] J. Rodríguez-López, N.L. Ritzert, J.A. Mann, C. Tan, W.R. Dichtel, H.D. Abruña, Quantification of the Surface Diffusion of Tripodal Binding Motifs on Graphene Using Scanning Electrochemical Microscopy, J. Am. Chem. Soc. 134 (2012) 6224−6236.

[38] V. Singh, D. Joung, L. Zhai, S. Das, S.I. Khondaker, S. Seal, Graphene based materials: Past, present and future, Prog. Mater. Sci. 56 (2011) 1178–1271.

[39] D. Li, M. B. Muller, S. Gilje, R.B. Kaner, G.G. Wallace, Processable aqueous dispersions of graphene nanosheets, Nat. Nanotechnol. 3 (2008) 101–105.

[40] S. Park, R.S. Ruoff, Chemical methods for the production of graphenes, Nat. Nanotechnol. 4 (2009) 217–224.

[41] D.R. Dreyer, S. Park, C.W. Bielawski, R.S. Ruoff, The chemistry of graphene oxide, Chem. Soc. Rev. 39 (2010) 228–240.

[42] L. Liu, C. Tan, J. Chai, S. Wu, A. Radko, H. Zhang, D. Mandler, Electrochemically "Writing" Graphene from Graphene Oxide, Small 10 (2014) 3555–3559.

[43] J. Azevedo, L. Fillaud, C. Bourdillon, J.-M. Noël, F. Kanoufi, B. Jousselme, V. Derycke, S. Campidelli, R. Cornut, Localized Reduction of Graphene Oxide by Electrogenerated Naphthalene Radical Anions and Subsequent Diazonium Electrografting, J. Am. Chem. Soc. 136 (2014) 4833−4836.

[44] K. Torbensen, M. Kongsfelt, K. Shimizu, E.B. Pedersen, T. Skrydstrup, S.U. Pedersen, K. Daasbjerg, Patterned Carboxylation of Graphene Using Scanning Electrochemical Microscopy, Langmuir 31 (2015) 4443−4452.

[45] X.-K. Kong, C.-L. Chen, Q.-W. Chen, Doped graphene for metal-free catalysis, Chem. Soc. Rev. 43 (2014) 2841−2857.

[46] W. Zhang, L. Wu, Z. Li, Y. Liu, Doped graphene: synthesis, properties and bioanalysis, RSC Adv. 5 (2015) 49521–49533.

[47] J. Duan, S. Chen, M. Jaroniec, S.Z. Qiao, Heteroatom-Doped Graphene-Based Materials for Energy-Relevant Electrocatalytic Processes, ACS Catal. 5 (2015) 5207−5234.

[48] H. Fei, J. Dong, M.J. Arellano-Jiménez, G. Ye, N.D. Kim, E.L.G. Samuel, Z. Peng, Z. Zhu, F. Qin, J. Bao, M.J. Yacaman, P.M. Ajayan, D. Chen, J.M. Tour, Atomic cobalt on nitrogen-doped graphene for hydrogen generation, Nat. Commun. 6 (2015) 8668.

[49] X. Wang, G. Sun, P. Routh, D.-H. Kim, W. Huang, P. Chen, Heteroatom-doped graphene materials: syntheses, properties and applications, Chem. Soc. Rev. 43 (2014) 7067−7098.

[50] F. Bonaccorso, A. Lombardo, T. Hasan, Z. Sun, L. Colombo, A.C. Ferrari, Production and processing of graphene and 2d crystals, Mater. Today 15 (2012) 564−589.

[51] M.C.Z. Liu, H. Zhang, Two-dimensional transition metal dichalcogenide (TMD) nanosheets, Chem. Soc. Rev. 44 (2015) 2584−2586.

[52] X. Duan, C. Wang, A. Pan, R. Yu, X. Duan, Two-dimensional transition metal dichalcogenides as atomically thin semiconductors: opportunities and challenges, Chem. Soc. Rev. 44 (2015) 8859−8876.

[53] C. Tan, H. Zhang, Two-dimensional transition metal dichalcogenide nanosheet-based composites, Chem. Soc. Rev. 44 (2015) 2713−2731.

Figure captions

Fig. 1. Feedback mode of SECM operations. (A) the UME tip is far from the substrate. (B) positive feedback; species R is regenerated at the substrate. (C) Negative feedback: diffusion of R to the tip is hindered by the substrate. Reproduced from Ref 14 with permission of The Royal Society of Chemistry.

Fig. 2. Schematic representation of modes of operation (A) TG/SC and (B) SG/TC. Reproduced from Ref 14 with permission of The Royal Society of Chemistry.

Fig. 3. Micrographs of (a) PES-1G (×10,000), (b) PES-1G (×10,000), (c) PES-4G (×100) and (d) PES-4G (×2000). Reprinted from Electrochimica Acta, 93, J. Molina, J. Fernández, J.C. Inés, A.I. del Río, J. Bonastre, F. Cases, Electrochemical characterization of reduced graphene oxide-coated polyester fabrics, 44–52, Copyright (2013), with permission from Elsevier [18].

Fig. 4. Approach curves for: (a) PES (- - -), PES-GO (continuous lines) and theoretical negative feedback model (Δ). (b) PES-1G, PES-2G, PES-3G, PES-4G. Theoretical positive feedback (limit model) is also presented for comparison (Δ). Obtained with a 100 μm diameter Pt tip in 0.01 M $Fe(CN)_6^{3-}$ and 0.1 M KCl. The tip potential was 0 mV (vs Ag/AgCl) and the approach rate was 10 $\mu m \cdot s^{-1}$. Reprinted from Applied Surface Science, 279, J. Molina, J. Fernández, A.I. del Río, J. Bonastre, F. Cases, Chemical and electrochemical study of fabrics coated with reduced graphene oxide, 46–54, Copyright (2013), with permission from Elsevier [19].

Fig. 5. 3D (a) and 2D (b) constant height SECM images of: PES-4G sample. 0.25 cm^2 geometrical area sample, images were taken with a 100 μm diameter Pt tip, in 0.01 M $Fe(CN)_6^{4-}$ and 0.1 M KCl at a constant height. The tip potential was +400 mV, the scan rate was 200 $\mu m \cdot s^{-1}$ in comb mode; lengths of x and y lines were 1500 μm × 1500 μm with increments of 50 μm. Reprinted from Applied Surface Science, 279, J. Molina, J. Fernández, A.I. del Río, J. Bonastre, F. Cases, Chemical and electrochemical study of fabrics coated with reduced graphene oxide, 46–54, Copyright (2013), with permission from Elsevier [19].

Fig. 6. 2D SECM representations for Pt/RGO wires obtained by vertical displacement of the microelectrode for the different redox systems 0.01 M $Ru(NH_3)_6^{3+}$/0.1 KCl (a), 0.01 M $Fe(CN)_6^{3-}$/0.1 M KCl (b) and 0.02 M Fe^{3+}/0.5 M H_2SO_4 (c). Theoretical positive feedback model has been included as a black continuous line. Data obtained with a 25 mm diameter Pt tip, approach rate 10 $\mu m \cdot s^{-1}$. Reprinted from Electrochimica Acta, 166, J. Molina, J. Fernández, C. García, A.I. del Río, J. Bonastre, F. Cases, Electrochemical

characterization of electrochemically reduced graphene coatings on platinum. Electrochemical study of dye adsorption, 54–63, Copyright (2015), with permission from Elsevier [23].

Fig. 7. Area scans with a 12 μm radius probe (RG = 3) and a probe-substrate distance during the scans of 12 μm (L = 1); before and after exposure of GO on SiO_2/Si substrates to a pH = 13 solution using both FcMeOH and $FcMeOH^+$ ($FcMeOH^+$ was produced by electrolysis of FcMeOH). (a) and (b): before exposure, (a) tip current and (b) corresponding σe according to eq 6 and 3 ($i_{T,sol}$ = 0.43 nA). (c) and (d): after 30 s exposure, (c) tip current and (d) corresponding σe ($i_{T,sol}$ = 1.21 nA). The scanned zones are not the same in the two data sets. Reprinted with permission from (A.J. Wain, A.J. Pollard, C. Richter, High-Resolution Electrochemical and Topographical Imaging Using Batch-Fabricated Cantilever Probes, Anal. Chem. 86 (2014) 5143−5149). Copyright (2014) American Chemical Society [24].

Fig. 8. Feedback mode SECM-AFM images of exfoliated graphene/graphite flakes immersed in 1 mM FcMeOH/0.1 M KNO_3 solution: Topography is shown in (a), (c), (e), and (g) and the corresponding electrochemical scans are depicted in (b), (d), (f), and (h), respectively. Line scan profiles for parts (g) and (h) are shown in (i) (shaded areas highlight regions of different graphene thickness: single-layer (SL), multilayer (ML), and few-layer (FL). Tip bias 0.3 V vs Ag, line scan frequency 0.5 Hz, lift height 150 nm, bulk tip current typically ∼200 pA. Reprinted with permission from (A.J. Wain, A.J. Pollard, C. Richter, High-Resolution Electrochemical and Topographical Imaging Using Batch-Fabricated Cantilever Probes, Anal. Chem. 86 (2014) 5143−5149). Copyright (2014) American Chemical Society [25].

Fig. 9. Image of an agglomerate of r-GO flakes deposited on Si-SiO_2 substrate obtained by (a) SEM at 15 kV and (b) SECM. [Fc] = 0.04 mM, rT = 5 μm. The color scale represents the probe current increase normalized to the bulk probe current (0.07 nA). (c) Schematic representation of the electronic pathway occurring during SECM feedback measurements when the flakes are in contact. Reprinted with permission from (T. Bourgeteau, S.L. Vot, M. Bertucchi, V. Derycke, B. Jousselme, S. Campidelli, R. Cornut, New Insights into the Electronic Transport of Reduced Graphene Oxide Using Scanning Electrochemical Microscopy, J. Phys. Chem. Lett. 5 (2014) 4162−4166). Copyright (2014) American Chemical Society [27].

Fig. 10. SECM response obtained with a redox Fc mediator concentration of (a) 0.25, (b) 0.8, and (c) 15 mM. The color scale represents the probe current increase normalized by the bulk probe current (I_{inf}) ((a):0.44, (b): 1.28, and (c): 25 nA). Reprinted with permission from (T. Bourgeteau, S.L. Vot, M. Bertucchi, V. Derycke, B. Jousselme, S. Campidelli, R. Cornut, New Insights into the Electronic Transport of Reduced Graphene Oxide Using Scanning Electrochemical Microscopy, J. Phys. Chem. Lett. 5 (2014) 4162−4166). Copyright (2014) American Chemical Society [27].

Fig. 11. SECM images of a mechanically induced defect and its passivation: (a) schematic of a mechanically induced defect (not to scale) on the graphene electrode; (b) SECM image of graphene with mechanically induced defect; (c) mechanically induced defect four cycles of o-phenylenediamine (OPD) electropolymerization. SECM tip, Pt radius= 7.5 μm biased at -0.1 V vs Ag/AgCl; graphene electrode, biased at +0.8 V vs Ag/AgCl; mediator, 2 mM $K_3(CN)_6$; electrolyte, 0.2 M PBS. Reprinted with permission

from (C. Tan, J. Rodríguez-López, J.J. Parks, N.L. Ritzert, D.C. Ralph, H.D. Abruña, Reactivity of Monolayer Chemical Vapor Deposited Graphene Imperfections Studied Using Scanning Electrochemical Microscopy, ACS Nano 6 (2012) 3070–3079). Copyright (2021) American Chemical Society [29].

Fig. 12. SECM images of a chemically induce defect and its passivation: (a) chemically induced defect using NaOCl; (b) Chemically induced defect after a total of four cycles of OPD electropolymerization. Chemically induced defects were induced by droplets of 10 mM NaOCl. SECM tip, Pt radius= 7.5 μm biased at -0.1 V vs Ag/AgCl; graphene electrode, biased at 0.8 V vs Ag/AgCl; mediator, 2 mM $K_3(CN)_6$; electrolyte, 0.2 M PBS. Reprinted with permission from (C. Tan, J. Rodríguez-López, J.J. Parks, N.L. Ritzert, D.C. Ralph, H.D. Abruña, Reactivity of Monolayer Chemical Vapor Deposited Graphene Imperfections Studied Using Scanning Electrochemical Microscopy, ACS Nano 6 (2012) 3070–3079). Copyright (2021) American Chemical Society [29].

Fig. 13. Nanogap voltammetry of the A) oxidation and B) reduction of the FcMeOH couple at a graphene electrode. Reprinted from, R. Chen, N. Nioradze, P. Santhosh, Z. Li, S.P. Surwade, G.J. Shenoy, D.G. Parobek, M.A. Kim, H. Liu, S. Amemiya, Ultrafast Electron Transfer Kinetics of Graphene Grown by Chemical Vapor Deposition, Angew. Chem. Int. Ed. 54 (2015) 15134–15137, with permission from Wiley-VCH Verlag GmbH & Co. © 2015 Wiley-VCH Verlag GmbH & Co. KGaA, Weinheim [34].

Fig. 14. Cyclic voltammograms for 10 mediators with corresponding $E_{1/2}$ (vs Ag/AgCl) values at a platinum ultramicroelectrode; a = 7.5 μm. Current was normalized to the steady-state current. Solutions of hexacyanoruthenate and octacyanomalybdate were at

2 mM in 0.1 M potassium chloride. Two millimolar iron ethylenediaminetetraacetic acid was used in 0.2 M phosphate buffer, pH 7, with 2 mM disodium ethylenediaminetetraacetic acid. All other mediators were at 1 mM with phosphate buffer or 0.1 M potassium chloride as supporting electrolyte. Sweep rate, 20 or 50 mV/s. Names for chemical formulae are the same as those in the footnote of Table 1. Reprinted with permission from (N.L. Ritzert, J. Rodríguez-López, C. Tan, H.D. Abruña, Kinetics of Interfacial Electron Transfer at Single-Layer Graphene Electrodes in Aqueous and Nonaqueous Solutions, Langmuir 29 (2013) 1683−1694). Copyright (2013) American Chemical Society [36].

Fig. 15. Electrochemically patterned graphene lines at different potentials: (A) SEM image; (B) magnified SEM image; (C) EDX mapping of carbon and (D) EDX mapping of oxygen. Line (1): −4.0 V; Line (2): −4.5 V; Line (3): −5.0 V (E surf vs. Etip). The scan rate of microelectrode is 2 μm/s. The microelectrode scans for 400, 450 and 500 μm for line (1), (2), and (3), respectively. Reprinted from, Liang Liu, Chaoliang Tan, Jianwei Chai, Shixin Wu, Anna Radko, Hua Zhang, Daniel Mandler, Electrochemically "Writing" Graphene from Graphene Oxide, Small 10 (2014) 3555–3559, with permission from Wiley-VCH Verlag GmbH & Co. © 2013 Wiley-VCH Verlag GmbH & Co. KGaA, Weinheim [42].

Fig. 16. SECM image of electrochemically patterned graphene lines. Line (1): 10 μm/s; (2): 15 μm/s; (3): 20 μm/s. E surf = −4.5 V vs. E tip. The electrolyte consisted of 1 mM dopamine, 0.1 M KCl and 0.1 M $HClO_4$. A 25 μm diameter Pt microelectrode (0.8 V vs. Ag/AgBr QRE) was approached to ca. 7 μm above the sample surface, and scanned at 20 μm/s. The microelectrode scans for 350, 400, 450 μ m for line (1), (2), (3) and (4),

respectively. Reprinted from, Liang Liu, Chaoliang Tan, Jianwei Chai, Shixin Wu, Anna Radko, Hua Zhang, Daniel Mandler, Electrochemically "Writing" Graphene from Graphene Oxide, Small 10 (2014) 3555–3559, with permission from Wiley-VCH Verlag GmbH & Co. © 2013 Wiley-VCH Verlag GmbH & Co. KGaA, Weinheim [42].

Fig. 17. (a) SEM image (0.5 kV) of a reduced line between two gold connection lines obtained after a displacement at 50 μm/s with a microelectrode having a radius of 5 μm, placed at about 10 μm from the substrate. [Naphthalene] = 50 mM. AFM image (b) and SEM at 30 kV images (c,d) obtained after electrografting of 4-aminoethylbenzenediazonium and exposition to a 5 nm gold nanoparticles suspension. AFM scale: 0−200 nm in thickness. Reprinted with permission from (J. Azevedo, L. Fillaud, C. Bourdillon, J.-M. Noël, F. Kanoufi, B. Jousselme, V. Derycke, S. Campidelli, R. Cornut, Localized Reduction of Graphene Oxide by Electrogenerated Naphthalene Radical Anions and Subsequent Diazonium Electrografting, J. Am. Chem. Soc. 136 (2014) 4833−4836). Copyright (2015) American Chemical Society [43].

Fig. 18. (A) SECM mapping of the Ni−Gra−5, Ni−Gra−10, and Ni−Gra−30 spots using 1 mM ferrocene as the redox probe in 0.1 M Bu4NBF4/MeCN. A homemade SECM platinum tip electrode (radius a= 12.5 μm and RG = 3) was used. The scale bar refers to the recorded tip current, i_T, normalized with respect to the bulk current, $i_{T,inf}$. (B) Line scans of Ni−Gra−5 (solid line), Ni−Gra−10 (dashed line), and Ni−Gra−30 (dotted line) using the SECM tip position during electrolysis as a reference point. Reprinted with permission from (K. Torbensen, M. Kongsfelt, K. Shimizu, E.B. Pedersen, T. Skrydstrup, S.U. Pedersen, K. Daasbjerg, Patterned Carboxylation of Graphene Using

Scanning Electrochemical Microscopy, Langmuir 31 (2015) 4443−4452). Copyright (2015) American Chemical Society [44].

Table captions

Table 1. Apparent heterogeneous electron transfer rate constants and diffusion coefficients for mediators in aqueous media. Reprinted with permission from (N.L. Ritzert, J. Rodríguez-López, C. Tan, H.D. Abruña, Kinetics of Interfacial Electron Transfer at Single-Layer Graphene Electrodes in Aqueous and Nonaqueous Solutions, Langmuir 29 (2013) 1683−1694). Copyright (2013) American Chemical Society [36].

Table 2. Electrode material, method of synthesis, SECM experimental conditions and application of the references analyzed related to graphene materials and SECM.

Table 1

Mediator[a]	$E_{1/2}$ (V vs Ag/AgCl)	k^0_{app} (cm/s)	D (cm^2/s)
Fe(III) EDTA	-0.2	5.4 (±2.2) x 10^{-4}	5 x 10^{-6}
$[Ru(CN)_6]^{4-}$	+0.67	7.5 (±1.2) x 10^{-4}	7 x 10^{-6}
$[Fe(CN)_6]^{4-}$	+0.18	9.5 (±7.9) x 10^{-4}	8 x 10^{-6}
$[Mo(CN)_8]^{4-}$	+0.52	1.4 (±0.8) x 10^{-3}	7 x 10^{-6}
$[Fe(CN)_6]^{3-}$	+0.18	1.9 (±0.4) x 10^{-3}	8 x 10^{-6}
CoSep	-0.65	4.5 (±3.9) x 10^{-3}	5 x 10^{-6}
FcMeOH	+0.22	2.0 (±0.4) x 10^{-2}	7 x 10^{-6}
MV	-0.65	>(2 x 10^{-2})	8 x 10^{-6}
$[Ru(NH_3)_6]^{3+}$	-0.26	>(2 x 10^{-2})	6 x 10^{-6}
$[Ru(bpy)_3]^{2+}$	+1.05	>(2 x 10^{-2})	5 x 10^{-6}

[a]Fe(III) EDTA is iron ethylenediaminetetracetic acid; $[Ru(CN)_6]^{4-}$ is hexacyanoruthenate (II); $[Fe(CN)_6]^{4-}$is hexacyanoferrate (II); $[Mo(CN)_8]^{4-}$ is octacyanomolybdate (IV); $[Fe(CN)_6]^{3-}$ is hexacyanoferrate (III); CoSep is cobalt (III) sepulchrate; FcMeOH is hydroxymethoxymethylferrocene; MV is methyl viologen; $[Ru(NH_3)_6]^{3+}$ is hexaammineruthenium; $[Ru(bpy)_3]^{2+}$ is tris(2,2'-bipyridyl)ruthenium-(II).

Table 2

Table 2. Electrode material, method of synthesis, SECM experimental conditions and application of the references analyzed related to graphene materials and SECM.

Electrode material	Method of synthesis of G film	SECM measurements	Application	Reference
GO-PES fabrics RGO-PES fabrics	Adsorption and reduction of GO on fabrics GO coating: 3 $g \cdot L^{-1}$ GO, 30 min GO reduction: 0.5 % wt. $Na_2S_2O_4$, 30 min, 90 ºC 1 to 4 RGO coatings applied	0.01 M $Ru(NH)_6^{3+}$ + 0.1 M KCl, microelectrode potential (-0.4 V), microelectrode diameter (Pt, 100 µm), approach rate (10 $\mu m \cdot s^{-1}$), WE potential (ocp), three-electrode configuration	Electroactivity	[18]
GO-PES fabrics RGO-PES fabrics	Adsorption and reduction of GO on fabrics GO coating: 3 $g \cdot L^{-1}$ GO, 30 min GO reduction: 0.5 % wt. $Na_2S_2O_4$, 30 min, 90 ºC 1 to 4 RGO coatings applied	0.01 M $Fe(CN)_6^{3-}$ + 0.1 M KCl (microelectrode potential, 0 V); 0.01 M $Fe(CN)_6^{3-}$ + 0.01 M $Fe(CN)_6^{4-}$ + 0.1 M KCl (microelectrode potential, 0 V or 0.4 V); 0.01 M $Ru(NH)_6^{3+}$ + 0.1 M KCl (microelectrode potential, -0.4 V); microelectrode diameter (Pt, 100 µm), approach rate (10 $\mu m \cdot s^{-1}$), WE potential (ocp), three-electrode configuration	Electroactivity	[19]
RGO-BSA-PES plasma trated fabrics RGO-PES fabrics	Adsorption and reduction of GO on fabrics Plasma treatment: 3000 $W \cdot min \cdot m^{-2}$ of plasma dosage applied BSA coating: 0.5 % wt. BSA solution, 10 min. Rinsing with water GO coating: 3 $g \cdot L^{-1}$ GO, 60 min GO reduction: 50 mM $Na_2S_2O_4$, 30 min, 90 ºC 1 to 10 RGO coatings applied on PES and 1 RGO coating applied on BSA-PES plasma trated fabrics	0.01 M $K_4Fe(CN)_6$ + 0.1 M KCl, microelectrode diameter (Pt, 100 µm), microelectrode potential (0 V vs. Ag/AgCl), approach rate (10 $\mu m \cdot s^{-1}$), WE potential (ocp), three-electrode configuration	Electroactivity	[20]
RGO-BSA-PES plasma trated fabrics TiO_2-RGO-BSA-PES plasma treated fabrics	Adsorption and reduction of GO on fabrics Plasma treatment: 3000 $W \cdot min \cdot m^{-2}$ of plasma dosage applied BSA coating: 0.5 % wt. BSA solution, 10 min. Rinsing with water GO coating: 3 $g \cdot L^{-1}$ GO, 60 min GO reduction: 50 mM $Na_2S_2O_4$, 30 min, 90 ºC 1 to 4 RGO coatings applied TiO_2 coating: 5 $g \cdot L^{-1}$ TiO_2 + Setamol BL (1 mL), 2 min, drying 100 ºC	0.01 M $K_4Fe(CN)_6$ + 0.1 M KCl, microelectrode diameter (Pt, 100 µm), microelectrode potential (0.4 V vs. Ag/AgCl), approach rate (10 $\mu m \cdot s^{-1}$), WE potential (ocp), three-electrode configuration Light irradiation of TiO_2/RGO coatings: 300 W, microelectrode located at 50 µm above the sample, variation of oxidation current at 0.4 V was registered vs. time	Electroactivity	[21]
PES-PPy/GO (fabrics) PPy/GO (powder pellets)	Chemical polymerization Solution: 0.02 M pyrrole + 10 %, 20% or 30 % GO respect to pyrrole mass, adsorption during 30 min on PES fabrics Reaction: Addition of 0.05 M $FeCl_3$ and reaction during 150 min	0.01 M $Ru(NH_3)_6^{3+}$/0.1 M KCl; or 0.02 M Fe^{3+}/0.5 M H_2SO_4, microelectrode potential (-0.4 V, and -0.1 V, respectively; vs. Ag/AgCl), microelectrode diameter (Pt, 25 µm or 100 µm), approach rate (10 $\mu m \cdot s^{-1}$), WE potential (ocp), three-electrode configuration	Electroactivity	[22]
ERGO/Pt	Electrochemical reduction Solution: 3 $g \cdot L^{-1}$ GO + 0.1 M $LiClO_4$. Synthesis of ERGO: CV between 0.6 V and -1.4 V at 50 $mV \cdot s^{-1}$ for 40 scans	0.01 M $Ru(NH_3)_6^{3+}$/0.1 M KCl; 0.01 M $Fe(CN)_6^{3-}$/0.1 M KCl and 0.02 M Fe^{3+}/0.5 M H_2SO_4, microelectrode potential (-0.4 V, 0 V and -0.1 V, respectively; vs. Ag/AgCl), microelectrode diameter (Pt, 25 µm), approach rate (10 $\mu m \cdot s^{-1}$), WE potential (ocp), three-electrode configuration	Electroactivity	[23]
GO-SiO_2/Si RGO-SiO_2/Si	Bubble deposition method for GO (3-5 nm thickness), reduction of GO by 0.1 M KOH, 30 s – 120 s, and thermal annealing at 1 h, 150 º C, vacuum	Ferrocenedimethanol (FcMeOH) + 0.1 M KCl, microelectrode diameter (Pt, 24 µm), RG = 3, microelectrode potential (0.4 V vs. Ag/AgCl), WE potential (ocp), three-electrode configuration	Conductivity, electroactivity	[24]
G/SiO_2/Si	Exfoliation by Scotch tape method	1 mM FcMeOH + 0.1 M KNO_3, microelectrode diameter (Pt, 400 nm),	Topography,	[25]

		microelectrode potential (0.3 V vs. Ag), three-electrode configuration Lift mode, 150 nm lift, line scan rate 0.5 Hz	electroactivity	
RGO/SiO_2/Si	RGO coated SiO_2/Si substrates obtained by wet-chemical reduction of graphene oxide with hydrazine vapour	1 mM FcMeOH + 100 mM KCl, microelectrode diameter (Pt, 10 μm), microelectrode potential (+0.3 V vs. pseudo Ag/AgCl reference electrode), three-electrode configuration, surface-tip distance (60 nm)	Field effect transistor, electroactivity	[26]
RGO/SiO_2/Si	Bubble deposition method for GO, reduction by HI vapors	0.04 mM – 15 mM ferrocene in N,N-dimethylformamide, microelectrode diameter (Pt, 10 μm), microelectrode potential (0.4 V vs. Ag/AgCl), three electrode configuration, surface-tip distance (4 μm)	Conductivity, electroactivity	[27]
GO/Au RGO/SiO_x	GO spin coating from aqueous solution RGO obtained by thermal reduction of GO	1 mM FcMeOH or $Ru(NH_3)_6Cl_3$ or $K_4Fe(CN)_6$ in phosphate buffer solution (pH 7.4), microelectrode potential (0.185 V, -0.12 V and 0.18 V, respectively), microelectrode diameter (Pt, 10 μm), RG (10) Other redox mediators were also used: $Na_3[IrCl_6]$ and FcCOOH.	Electroactivity	[28]
G/SiO_2-Si	CVD synthesis of monolayer G on Cu foil. Wet transfer to Si substrate. During the transfer, 8% PMMA in anisole was spinned coated on top graphene at 4000 rpm for 60 s. Thereafter Cu was etched with a $FeCl_3$ solution. Mechanical effects were induced using a glass tip 20 μm radius. Chemical defects were created using microdroplets 50-100 μm of 10 mM NaOCl in water (pH=8). Electropolymerization of OPD on graphene was carried out by potential cycling between 0 and +0.8 V vs Ag/AgCl in an OPD solution (13.7 nM) and Na_2SO_4 (0.1 M).	$K_3(CN)_6$ between 1 and 2 mM in 0.2 M pH 7 phosphate buffer, Pt microelectrode radius of 7.5 μm, microelectrode potential (-0.1 V). Substrate potential 0.8 V vs. Ag/AgCl.	Electroactivity	[29]
G-PEDOT-FeHCF/Au	RGO coating: RGO obtained by hydrazine reduction of GO, drop casting on Au surface RGO/PEDOT/$Fe(CN)_6^{3-}$ film formation: 0.1 M KCl + 0.01 M EDOT + 0.1 M $K_3[Fe(CN)_6]$, CV between -0.6 V and 1.0 V at 50 $mV \cdot s^{-1}$, 10 scans, 50 $mV \cdot s^{-1}$ FeCHF film formation: 0.01 M $FeCl_3$ + 0.1 M KCl + 0.01 M HCl, CV between -0.2 V and 0.6 V at 50 $mV \cdot s^{-1}$, 10 scans, 50 $mV \cdot s^{-1}$	1 mM $Fe(CN_6)^{3-}$, microelectrode potential (-0.1 V vs. Ag/AgCl), substrate potential (+0.5 V vs. Ag/AgCl), microelectrode diameter (Pt, 10 μm), RG (5), substrate-tip distance > 200 μm, 4-electrode configuration	Electroactivity	[30]
G-PEDOT-FeHCF/Au	RGO/PEDOT/$Fe(CN)_6^{3-}$ film formation: 0.1 M KCl + 0.01 M EDOT + 0.1 M $K_3[Fe(CN)_6]$ + 2 g·L-1 RGO, CV between -0.6 V and 1.0 V at 50 $mV \cdot s^{-1}$, 10 scans, 50 $mV \cdot s^{-1}$ FeCHF film formation: 0.01 M $FeCl_3$ + 0.1 M KCl + 0.01 M HCl, CV between -0.2 V and 0.6 V at 50 $mV \cdot s^{-1}$, 10 scans, 50 $mV \cdot s^{-1}$	1 mM $Fe(CN_6)^{3-}$ + 0.1 M phosphate buffer solution, microelectrode potential (-0.1 V vs. Ag/AgCl), substrate potential (0.1 to 0.7 V vs. Ag/AgCl), microelectrode diameter (Pt, 10 μm), 4-electrode configuration, approaching rate 2.5 $\mu m \cdot s^{-1}$ H_2O_2 mapping: Generation-collection mode, microelectrode potential (-0.5 V), electrode potential (0 V), substrate-tip distance 50 μm	Electroactivity, rate constants	[31]
PPy/GO PPy/ERGO Pani/GO Pani/ERGO	Electrochemical polymerization of PPy or Pani Electrochemical reduction of GO to produce ERGO	10 mM FeMeOH + 1 M KCl, microelectrode potential (-0.1 V), substrate potential (0.4 or 0.2 V). Mode: Tip generation-substrate collection	Supercapacitors	[32]
MnO_2-GO/carbon fiber cloth MnO_2-RGO/carbon fiber cloth	GO/RGO deposition: Spray coating MnO_2 deposition: CV between -1.6 V and 0 V, 50 $mV \cdot s^{-1}$, 0.05 M $(CH_3COO)_2Mn \cdot 4H_2O$ + 0.1 M Na_2SO_4, mass loading (100 $\mu g \cdot cm^{-2}$)	10 mM $K_3Fe(CN)_6$ + 1 M KCl, microelectrode potential (-0.2 V), substrate potential (0.5 V), microelectrode diameter (10 μm), tip-substrate separation (40 μm)	Supercapacitors	[33]
G/polystyrene	CVD synthesis of G on Cu foil	Nanogap voltammetry. 0.5 mM FcMeOH + 1 M KCl, microelectrode	Rate constants	[34]

G/PMMA	Drop casting on one G side with PMMA or polystyrene Fixing on a PDMS support and attachment to a glass plate Etching of the copper foil and insulating of Cu exposed edges	diameter (Pt, 10 μm), RG (1), nanogap 30-450 nm k^0 G (Polystyrene): > 25 $cm \cdot s^{-1}$ k^0 G (PMMA): ~ 1.6 $cm \cdot s^{-1}$		
G-n-octadecyl mercaptan/Au	Coating of Au by n-octadecyl mercaptan (self-assembled monolayer), 4.0 mM $C_{18}H_{37}SH$, 24 h, room temperature Adsorption of G nanosheets on n-octadecyl mercaptan/Au, 1 $g \cdot L^{-1}$ G nanosheets in N,N-Dimethylformamide, 30 min	1.0 mM $Ru(NH_3)_6$ + 0.1 M PBS (pH 7.0), microelectrode potential (-0.5 V), substrate potential (0.1 V), microelectrode diameter (25 μm), RG (5), three-electrode cell	Rate constants	[35]
G-SiO_2/Si	CVD synthesis of G on Cu foil, PMMA layer to support G during transfer, Cu etching and PMMA etching, transfer to SiO_2/Si	Pt tip, RG (10). For reducing potentials a mercury film was applied to the Pt microelectrode to prevent side reactions	Rate constants	[36]
cobalt bis-terpyridine, Co(tpy)2-containing tripodal compound/G-SiO_2/Si	Synthesis and SECM study of a tripodal compound of a Co(II) bis-terpyridine [Co(tpy)2]redox center attached to a tetrahedral core bearing three pyrene feet that moieties interact strongly with the G surface	Microelectrode diameter (25 μm), RG (7), tip-substrate separation (10 μm) H_2O_2 collection: 0.2 M phosphate buffer solution, pH 7, air saturated, tip potential (0.6 V), substrate potential (-0.6 V) Feedback mode: Potassium ferricyanide (1-2 mM) + 0.2 M phosphate buffer, pH 7, tip potential (-0.1 V), substrate potential (0.4 V)	Diffusion coefficients	[37]
RGO/stainless steel	Electrochemical synthesis GO solution: 0.6 $g \cdot L^{-1}$ (500 nm, size flake), microelectrode diameter (Pt, 25 μm), reduction potential (-4.5 V, vs. tip), scan rate (10 $\mu m \cdot s^{-1}$), distance between substrate and microelectrode (~12 μm)	1 mM dopamine + 0.1 M KCl + 0.1 M $HClO_4$, microelectrode diameter (Pt, 25 μm), microelectrode potential (0.8 V vs. Ag/AgBr), distance between substrate and microelectrode (~12 μm), scan area (800 × 800 μm^2), scan rate (20 $\mu m \cdot s^{-1}$)	Patterning	[42]
RGO/SiO_2 AuNPs/4-aminoethylbenzenediazonium - RGO/SiO_2	Electrochemical reduction Solution: 80 mM/25 mM naphthalene, microelectrode diameter (10 μm/1 μm), reduction potential (-2.6 V vs. SCE), scan rate (100 $\mu m \cdot s^{-1}$/400 $\mu m \cdot s^{-1}$/1000 $\mu m \cdot s^{-1}$), distance between substrate and microelectrode (10 μm/3 μm) Electrografting of diazonium derivative: Immersion in a solution of protonated 4-aminoethylbenzenediazonium tetrafluoroborate (10^{-3} M). AuNPs modification: cyclic voltammetry between 0 V and -1 V at 100 $mV \cdot s^{-1}$ in a solution containing colloidal AuNPs.	1 mM Ferrocene, microelectrode diameter (10 μm), tip−substrate distance (10 μm).	Patterning	[43]
Multilayered CVD G/Ni-Si	CVD multilayered G on Ni substrate Solution: 0.1 M Bu_4NBF_4/DMF saturated with CO_2, and it was covered with a blanket of CO_2, microelectrode dimeter (Pt, 25 μm), distance between substrate and microelectrode (~13 μm). Electrolysis: -2.6 V, two electrode configuration. G electrode (WE), microelectrode (CE)	1 mM ferrocene + 0.1 M Bu_4NBF_4/MeCN, microelectrode diameter (Pt, 25 μm), microelectrode potential (0.7 V vs. Ag/Ag+), WE potential (ocp), three-electrode configuration	Patterning, carboxylation	[44]

Figure 1

Click here to download high resolution image

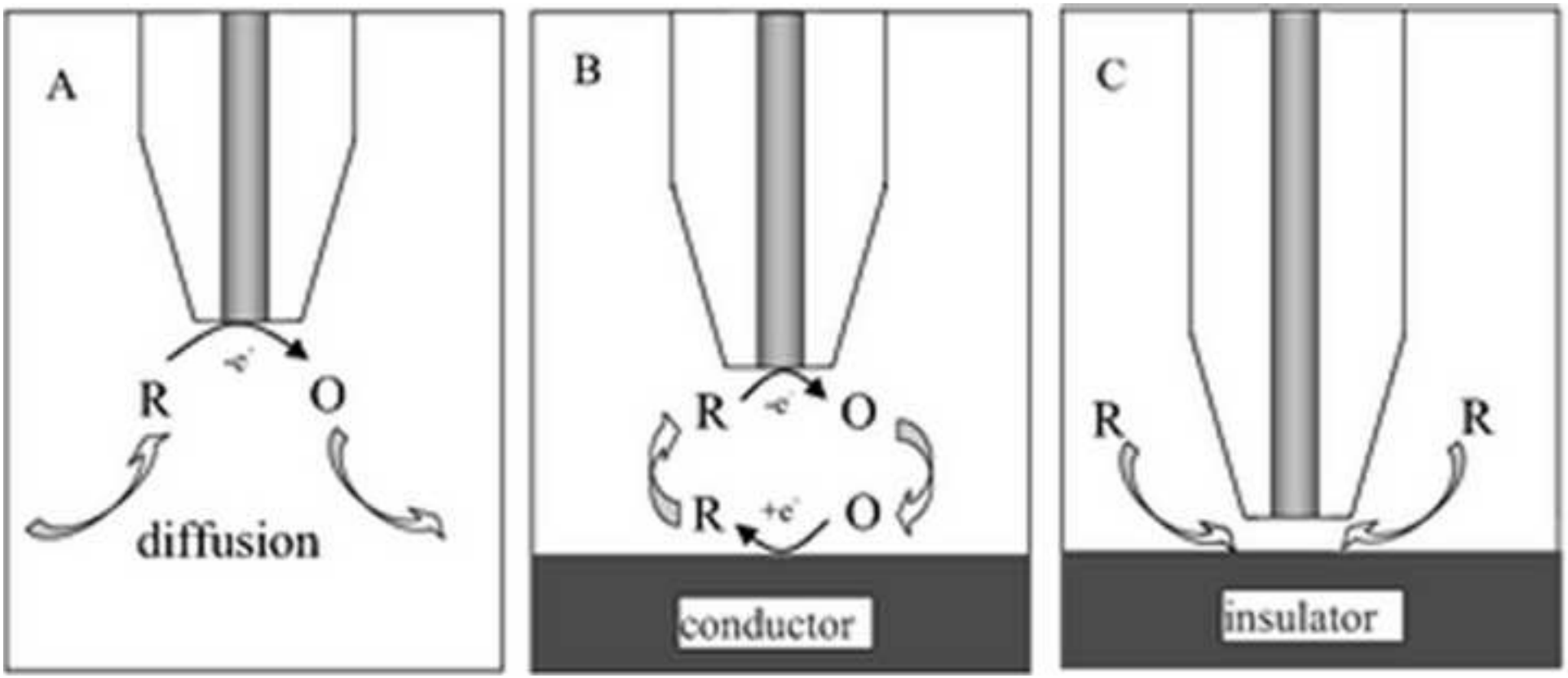

Figure 2

Click here to download high resolution image

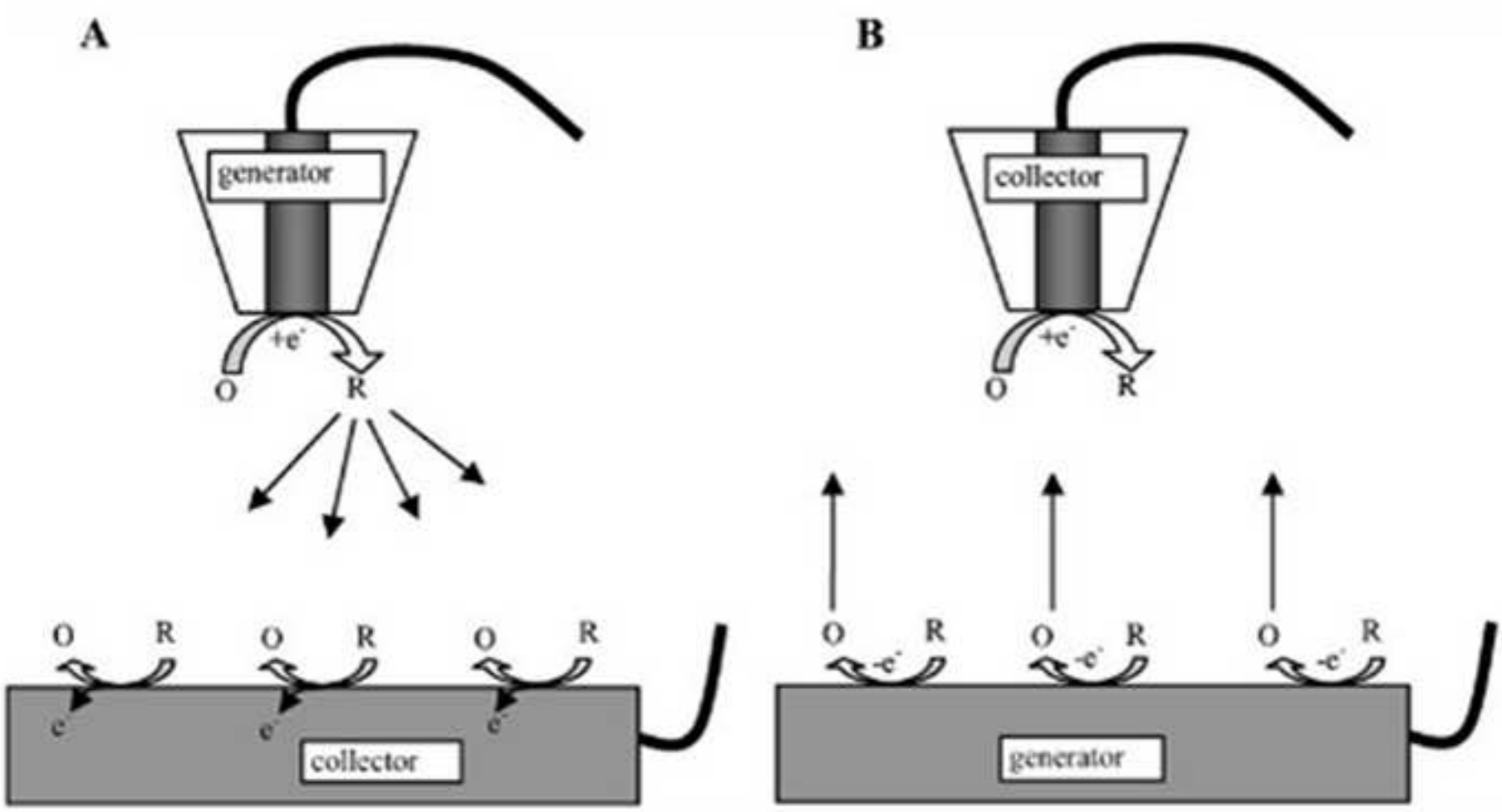

Figure 3

Click here to download high resolution image

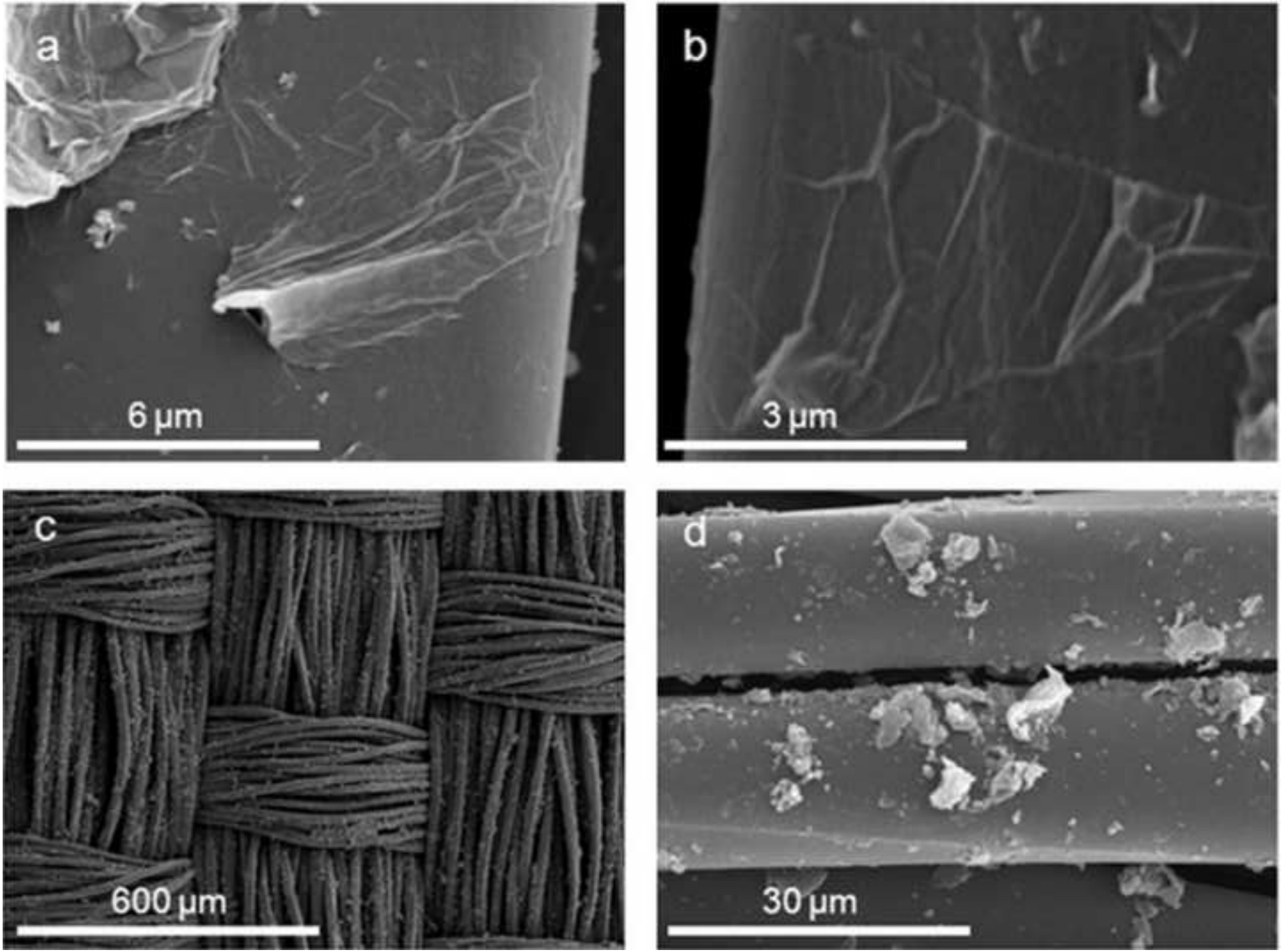

Figure 4

Click here to download high resolution image

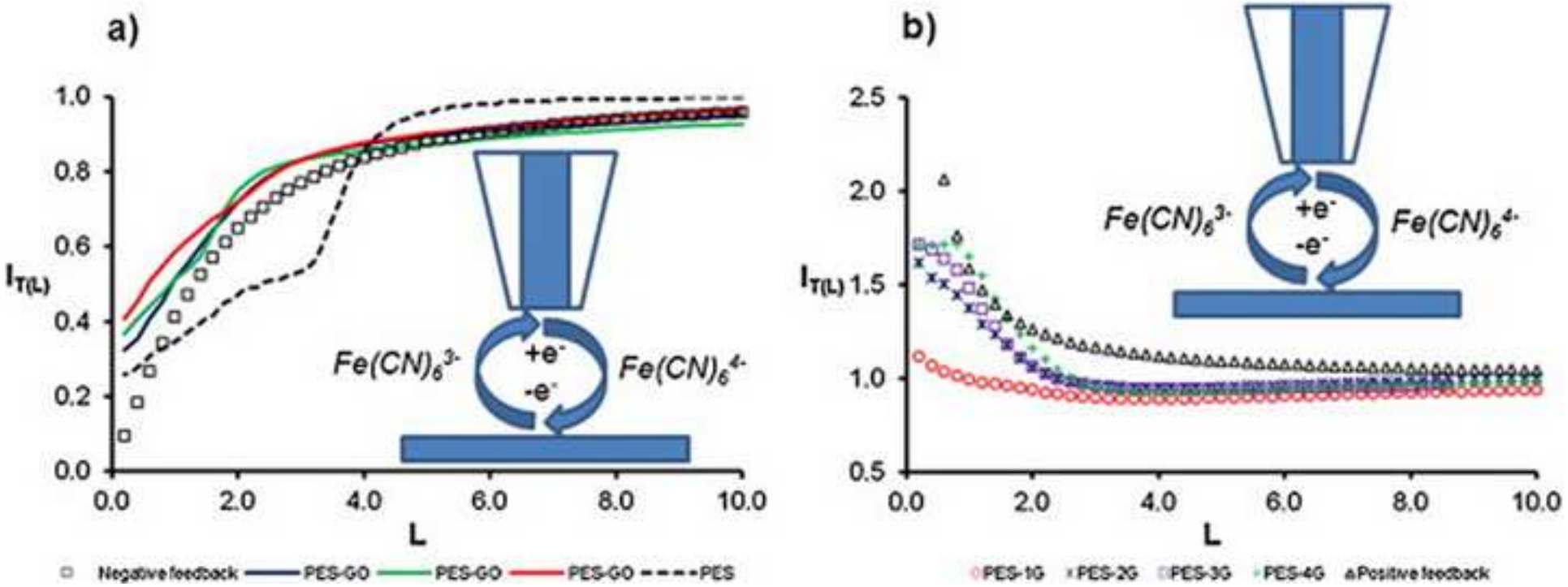

Figure 5

Click here to download high resolution image

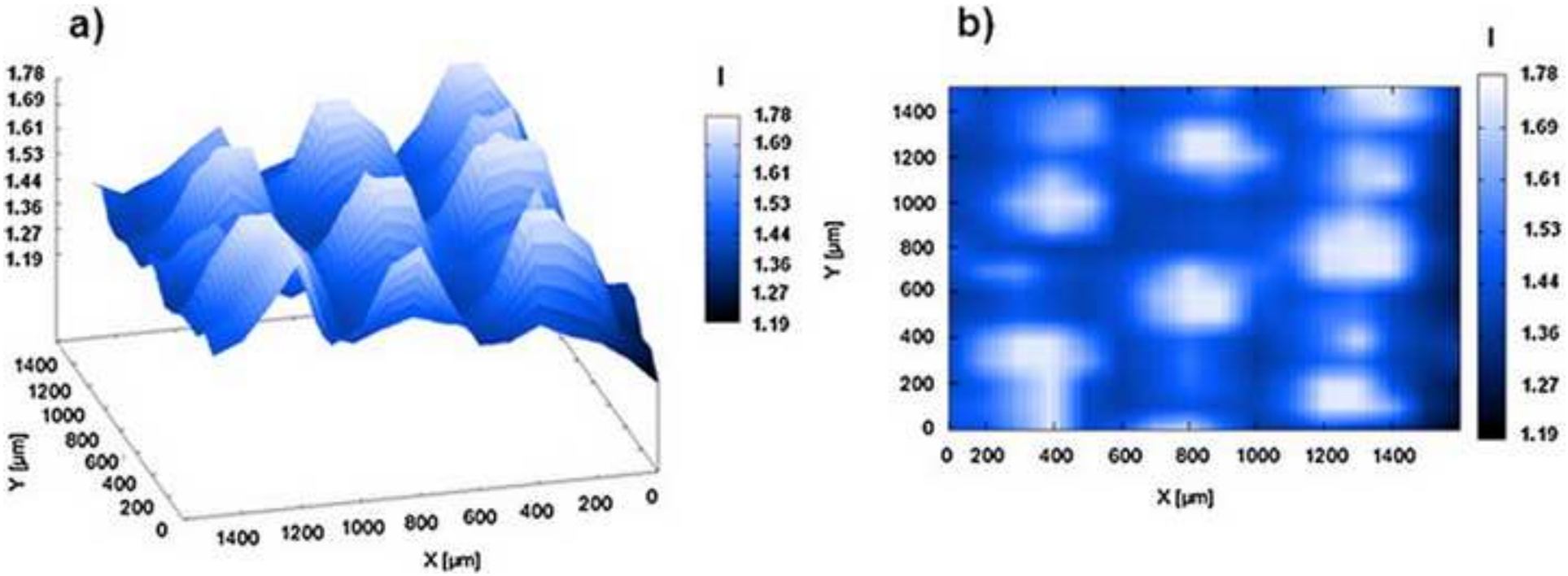

Figure 6

Click here to download high resolution image

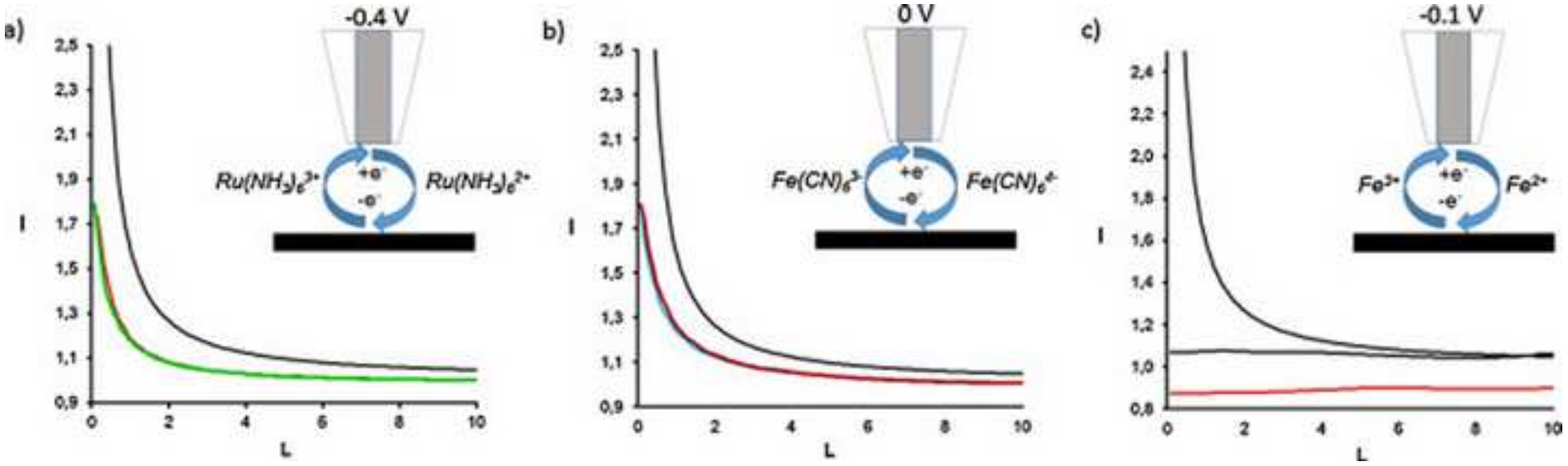

Figure 7

Click here to download high resolution image

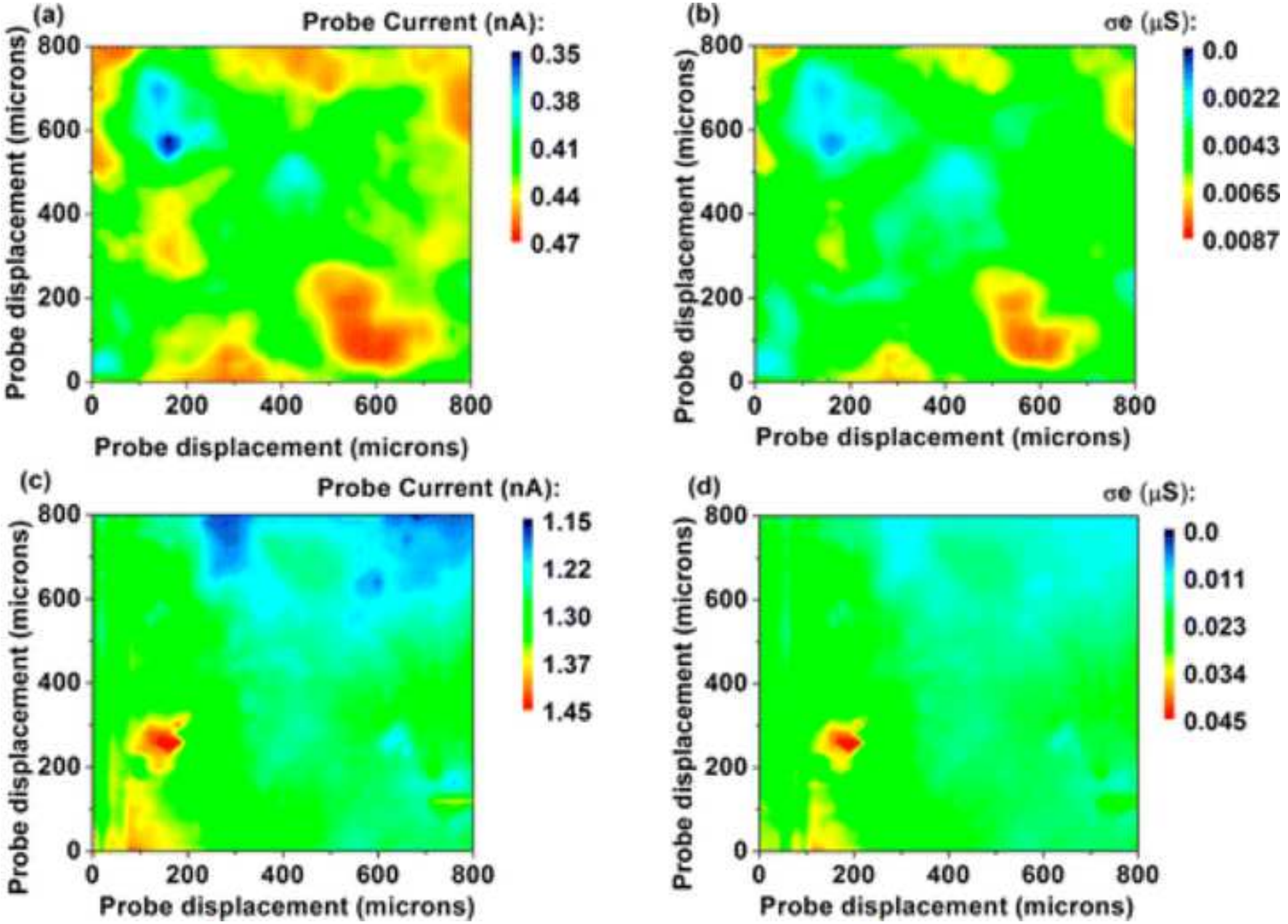

Figure 8

Click here to download high resolution image

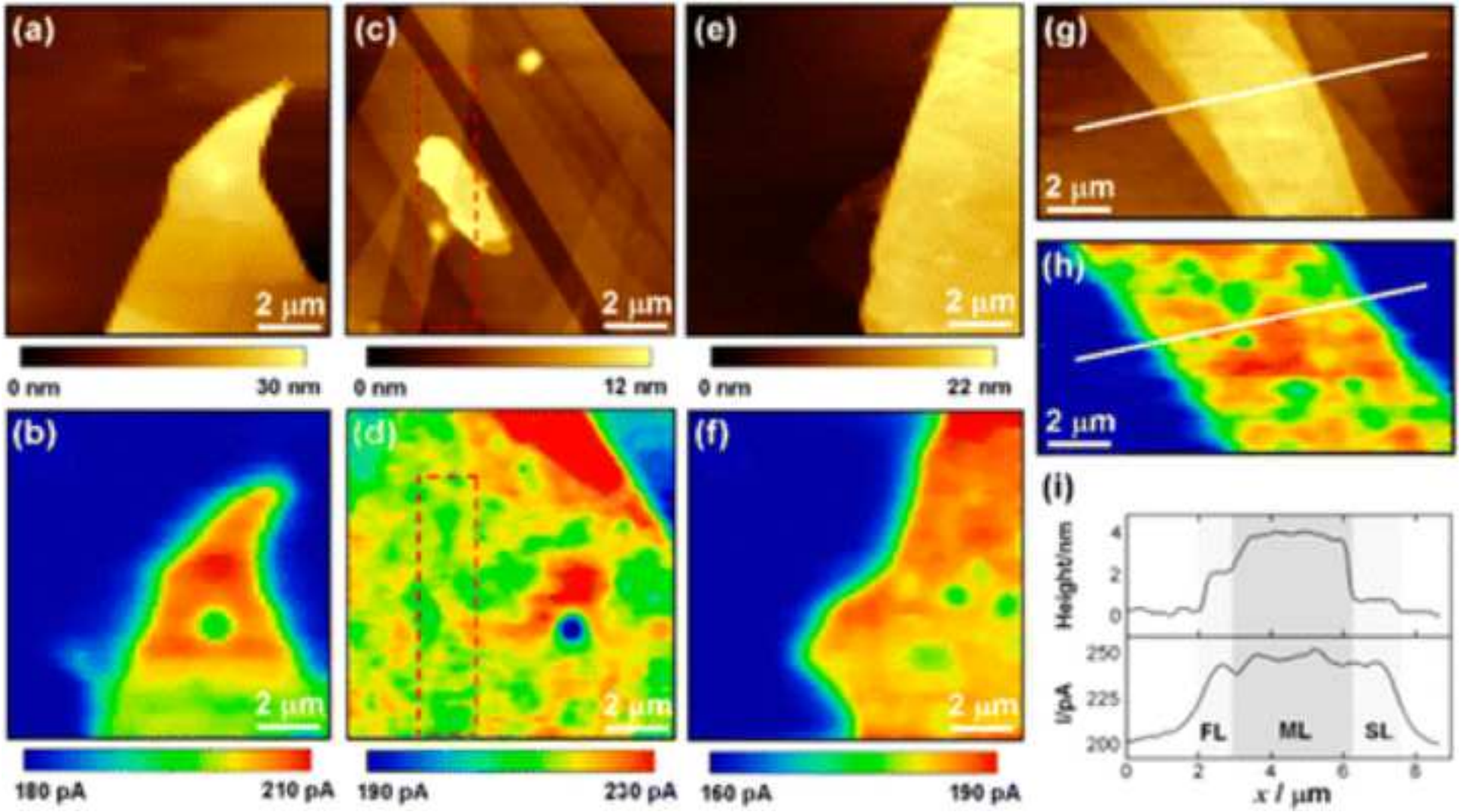

Figure 9

Click here to download high resolution image

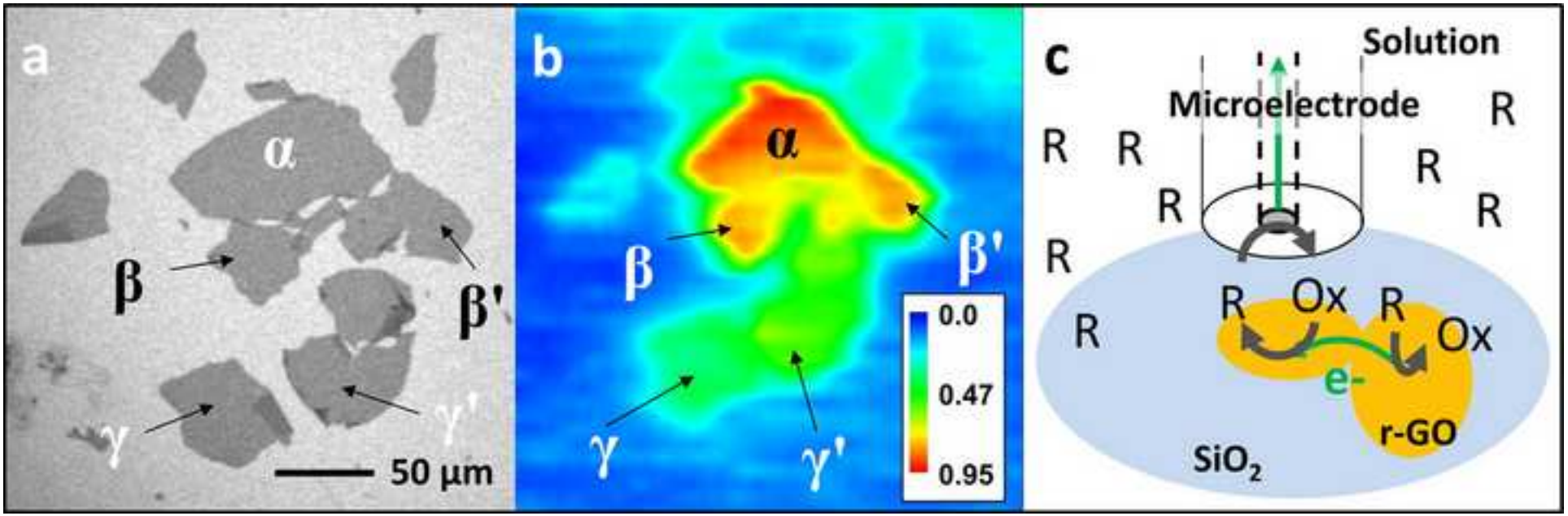

Figure 10

Click here to download high resolution image

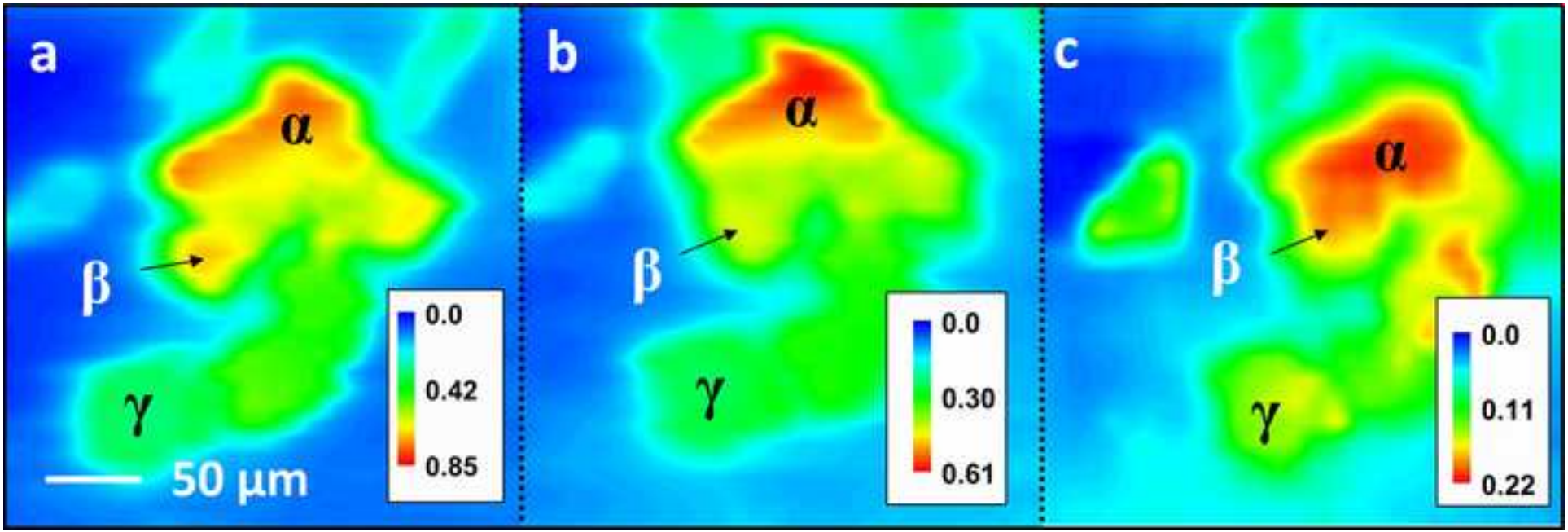

Figure 11

Click here to download high resolution image

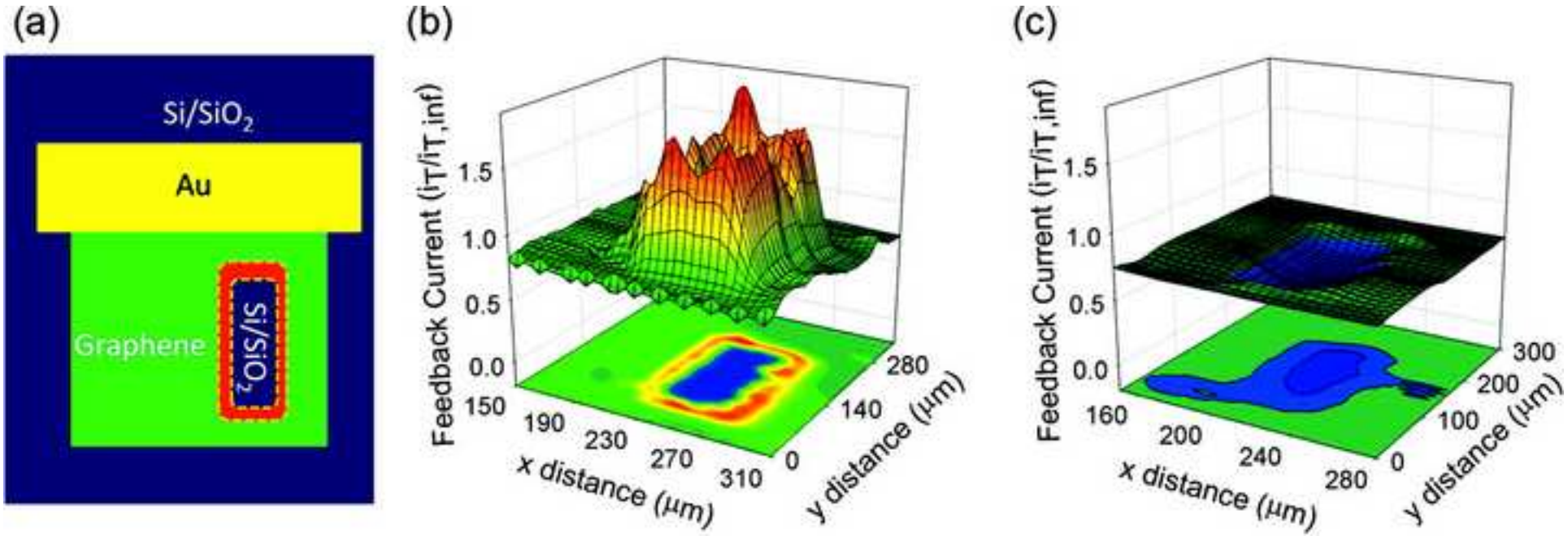

Figure 12

Click here to download high resolution image

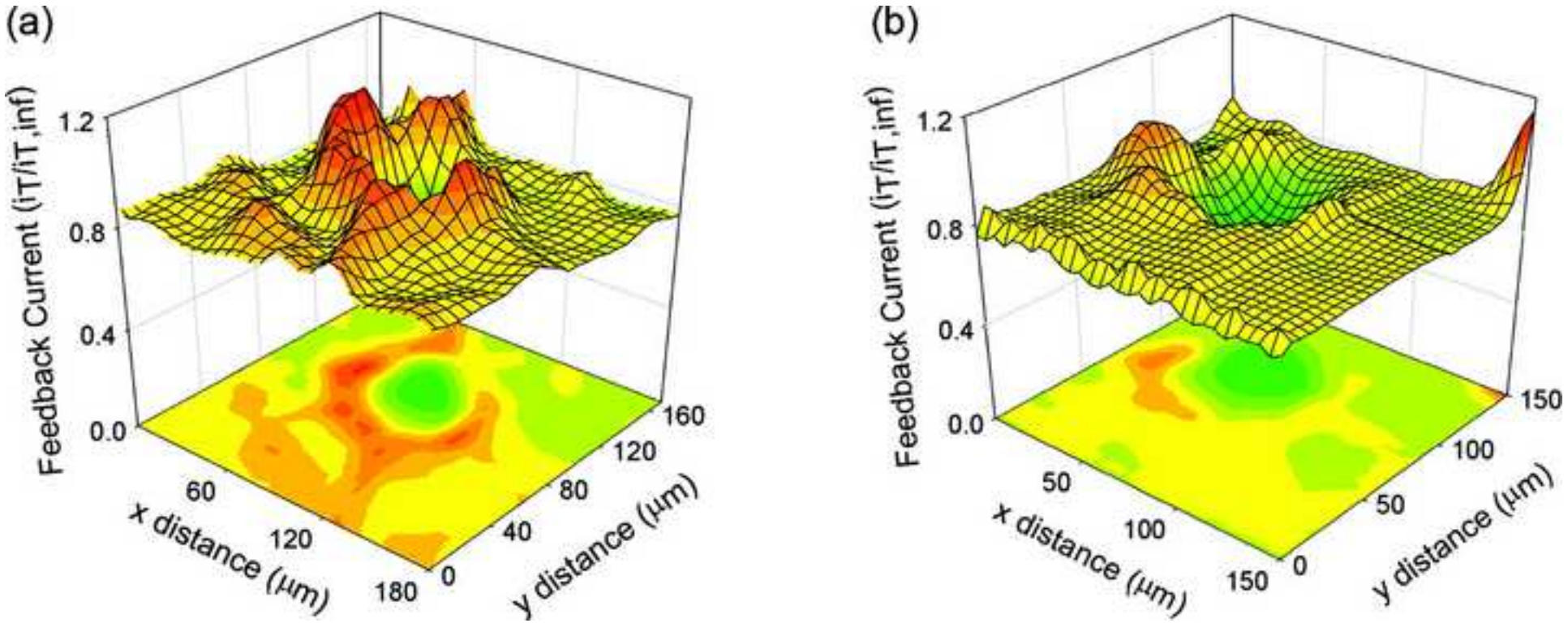

Figure 13
Click here to download high resolution image

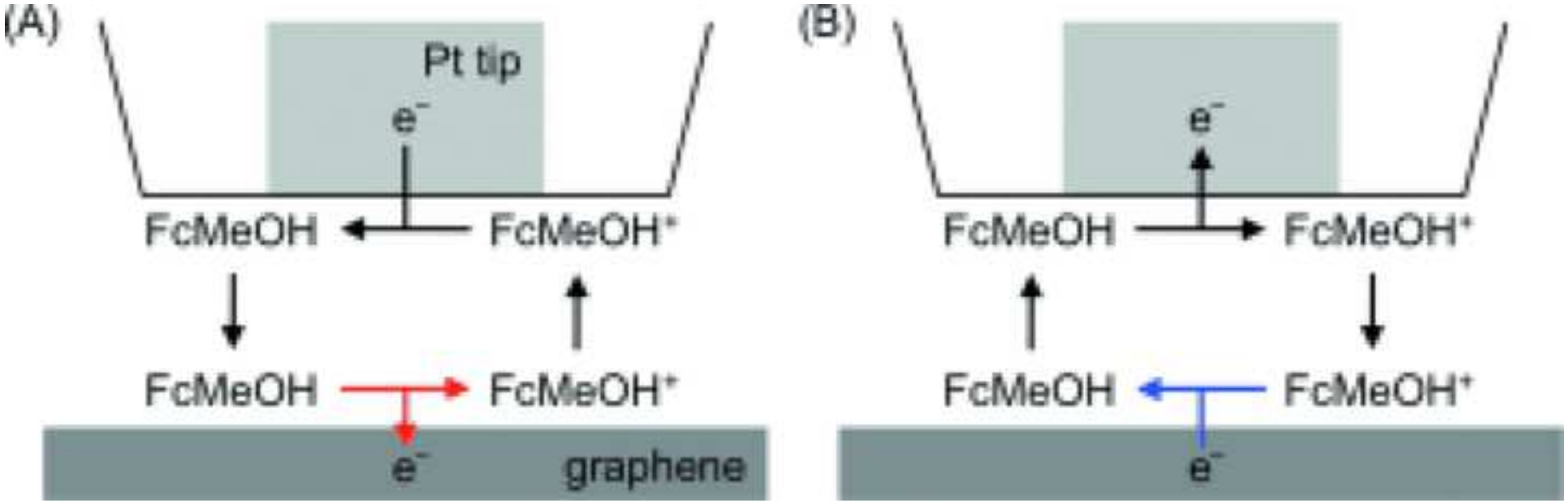

Figure 14

Click here to download high resolution image

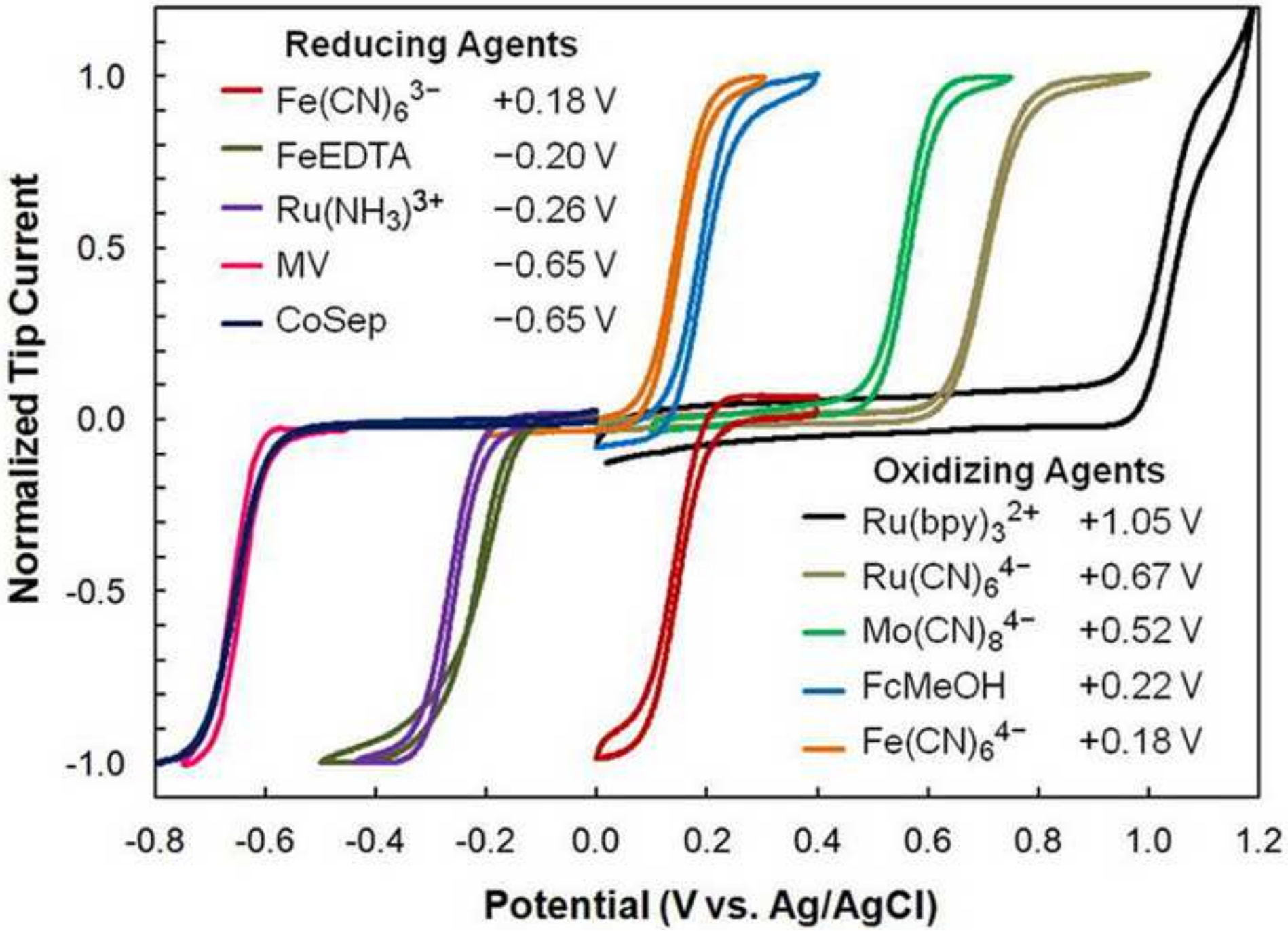

Figure 15
Click here to download high resolution image

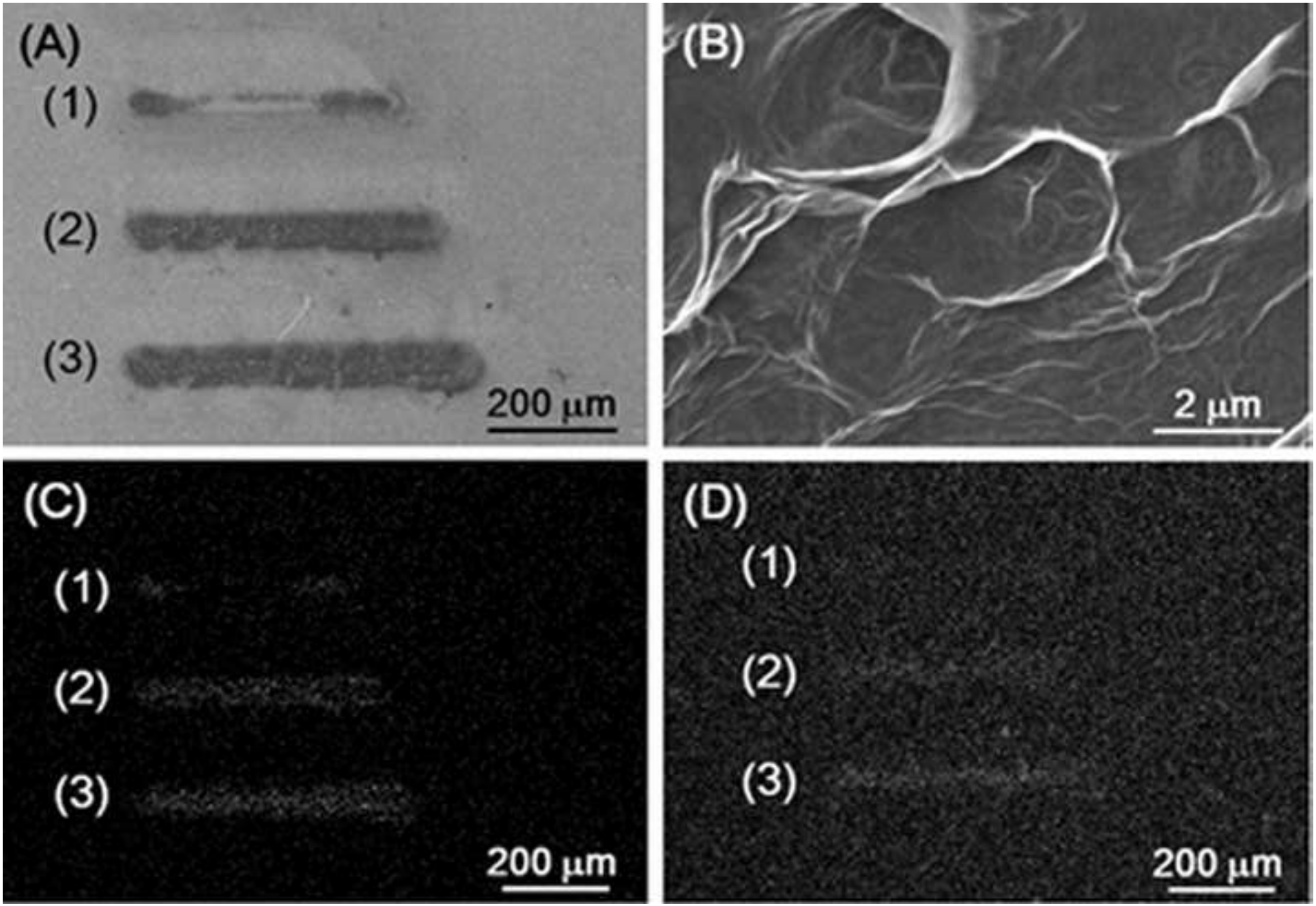

Figure 16
Click here to download high resolution image

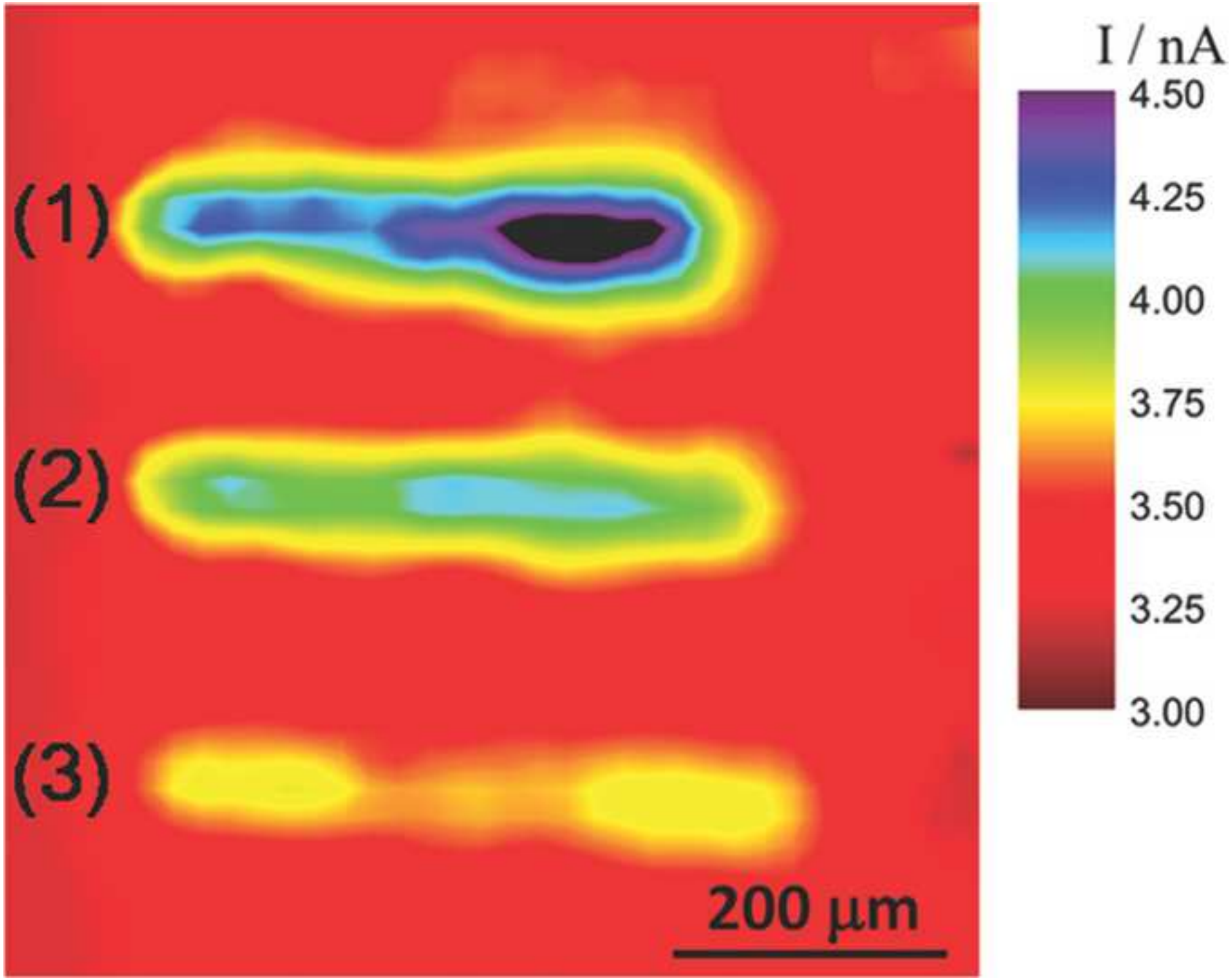

Figure 17

Click here to download high resolution image

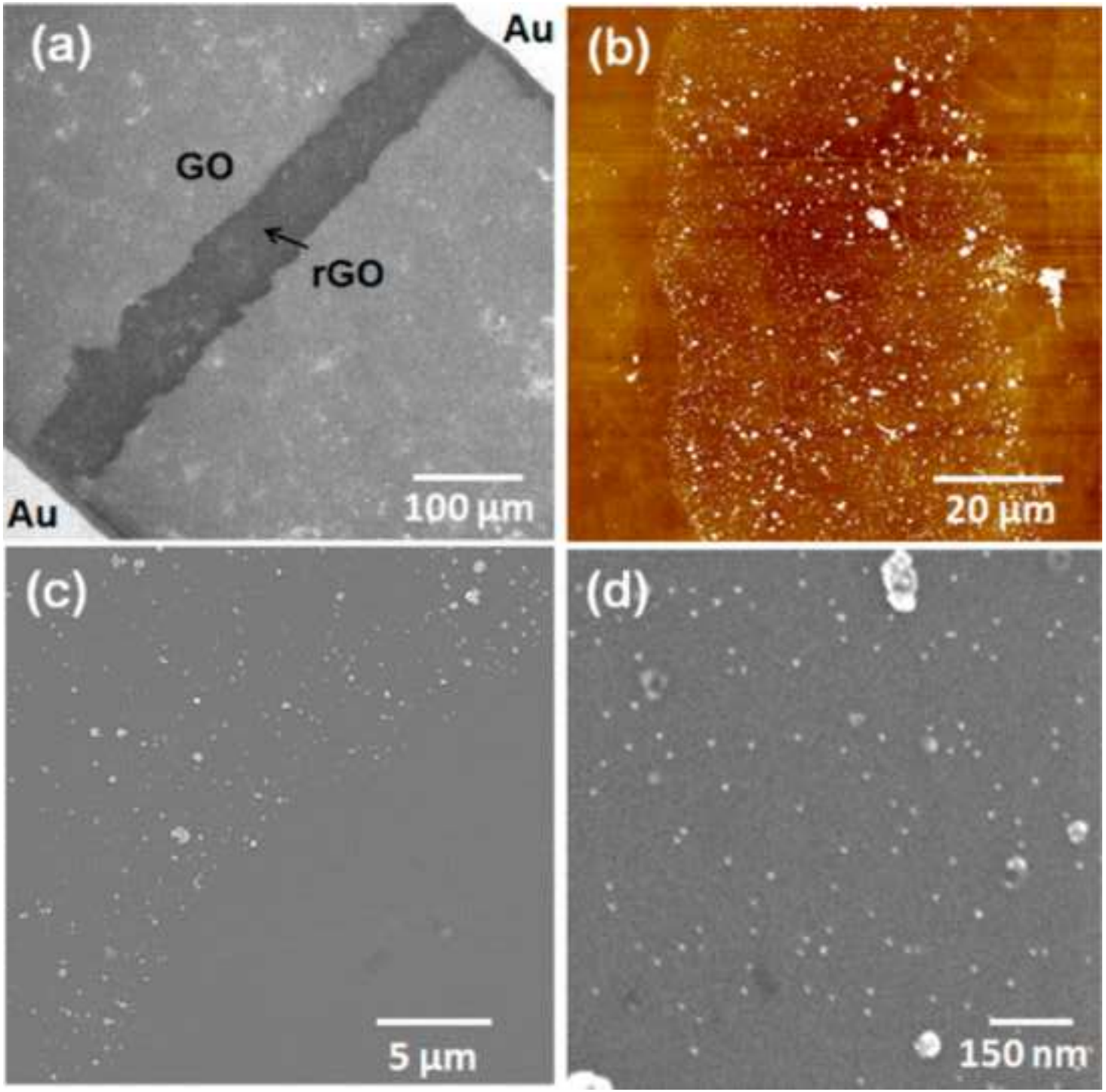

Figure 18
Click here to download high resolution image